ELSEVIER

Chemical Geology 231 (2006) 326–349

CHEMICAL GEOLOGY
INCLUDING
ISOTOPE GEOSCIENCE

www.elsevier.com/locate/chemgeo

UV–Vis spectrophotometric and XAFS studies of ferric chloride complexes in hyper-saline LiCl solutions at 25–90 °C

Weihua Liu [a,b], Barbara Etschmann [a], Joël Brugger [c,b,*], Leone Spiccia [d], Garry Foran [e], Brent McInnes [a]

[a] *CSIRO Exploration and Mining, P.O. Box 312, Clayton, VIC 3168, Australia*
[b] *South Australian Museum, North Terrace, Adelaide, SA 5000, Australia*
[c] *School of Earth and Environmental Sciences, University of Adelaide, Adelaide, SA 5005, Australia*
[d] *School of Chemistry, Monash University, Victoria 3800, Australia*
[e] *Australian National Beamline Facility, KEK, Photon Factory, Oho 1-1, Tsukuba-shi, Ibaraki-ken 305-0801, Japan*

Received 12 October 2004; received in revised form 6 October 2005; accepted 1 February 2006

Abstract

The speciation and thermodynamic properties of ferric chloride complexes in hydrothermal solutions and hypersaline brines are still poorly understood, despite the importance of this element as a micronutrient and ore-component. Available experimental data are limited to room temperature and relatively low chloride concentrations. This paper reports results of UV–Vis spectrophotometric and synchrotron XAFS experiments of ferric chloride complexes in chloride concentrations up to 15 m and at temperatures of 25–90 °C. Qualitative interpretation of the UV–Vis spectra shows that $FeCl^{2+}$, $FeCl_2^+$, $FeCl_{3(aq)}$ and $FeCl_4^-$ were present in the experimental solutions. As chloride concentrations increase, higher ligand number complexes become important with $FeCl_4^-$ predominating in solutions containing more than 10 m at 25 °C. The predominance fields of $FeCl_{3(aq)}$ and $FeCl_4^-$ expand to lower Cl concentrations with increasing *T*. Both XANES and UV–Vis spectra reveal a major change in the geometry of the complex between $FeCl_2^+$ and $FeCl_{3(aq)}$. EXAFS data confirm that the number of chloride ligands increases with increasing chloride concentration and show that Fe^{3+}, $FeCl^{2+}$ and $FeCl_2^+$ share an octahedral geometry. $FeCl_{3(aq)}$ could be either tetrahedral or trigonal dipyramidal, while $FeCl_4^-$ is expected to be tetrahedral. EXAFS data support a tetrahedral geometry for $FeCl_4^-$, especially at 90 °C, but do not allow to distinguish between a tetrahedral or trigonal dipyramidal geometry for $FeCl_{3(aq)}$ because of similar Fe–Cl distances. At room temperature, EXAFS data suggest that $FeCl_{3(aq)}$ may be a mixture of octahedral and tetrahedral or trigonal dipyramidal forms.

The room temperature formation constants for three ferric chloride complexes ($FeCl_2^+$, $FeCl_{3(aq)}$ and $FeCl_4^-$) determined from the UV data are generally in good agreement with previous studies. Calculations based on the properties extrapolated to 300 °C show that hematite solubility is much higher than previously estimated, and that the high orders complexes $FeCl_{3(aq)}$ and $FeCl_4^-$ are important at high temperatures even in solutions with low chloride concentrations. The accuracy of these properties is limited by a poor understanding of activity–composition relationships in concentrated electrolytes, and by limitations in the available experimental techniques and extrapolation algorithms; however, the inclusion of higher order complexes in numerical models of ore transport and deposition allows for a more accurate qualitative prediction of Fe behaviour in hydrothermal and hypersaline systems.

Keywords: Fe(III)-chloro complexes; UV–Vis spectrophotometry; XANES and EXAFS spectroscopy; Hypersaline brine; Hydrothermal ore deposits

* Corresponding author. South Australian Museum, North Terrace, Adelaide, SA 5000, Australia.
E-mail address: Joel.Brugger@adelaide.edu.au (J. Brugger).

0009-2541/$ - see front matter © 2006 Elsevier B.V. All rights reserved.
doi:10.1016/j.chemgeo.2006.02.005

1. Introduction

Iron is an important element in major and accessory minerals found in hydrothermal ore deposits that form over conditions ranging from diagenetic to exhalative to magmatic hydrothermal. Fe exists in minerals as Fe^{2+} (e.g., pyrite), Fe^{3+} (e.g., hematite) or in mixed valence states (e.g., magnetite). Fe is also an essential oligo-element controlling biomass in surface and ground waters (e.g., Millero et al., 1995). Many hydrothermal waters, as well as some shallow ground waters (e.g., playa lakes; semi-arid Australia, Peck and Hatton, 2003) contain salt concentrations much higher than that of seawater ($\gg 0.6$ m). Under acid drainage conditions, the concentration of Fe(III) operates a first order control on the rate of the acid production, Fe(III) acting as a catalyst to promote the oxidation of sulfide minerals. Hence, understanding the nature and stability of Fe(III)-chloro complexes over a wide range of chloride concentration and temperature is important for predicting Fe transport in ore-forming systems, and also its bioavailability in hypersaline environments.

Despite numerous studies on the nature and stability of ferric chloride complexes conducted using a variety of techniques including ultra-violet–visible (UV–Vis) and Raman spectroscopy, potentiometry, calorimetry and X-ray absorption fine structure spectrometry (XAFS) (e.g., Moller, 1937; Rabinowitch and Stockmayer, 1942; Friedman, 1952; Gamlen and Jordan, 1953; Marcus, 1960; Woods et al., 1962; Heistand and Clearfield, 1963; Rowley and Sutin, 1970; Rao and Rao, 1971; Byrne and Kester, 1976; Strahm et al., 1979; Byrne and Kester, 1981; Apted et al., 1985; Murata et al., 1989; Brubaker and Peterson, 1989; Millero et al., 1995; Inada and Funahashi, 1999; Tagirov et al., 2000), the speciation and standard thermodynamic properties of ferric chloride complexes in hypersaline solutions are still poorly understood. In acidic aqueous solution, Fe(III) exists as the hexa-aquo complex, $[Fe(OH_2)_6]^{3+}$, an ion with octahedral geometry (e.g., Harris et al., 1997). As the chloride concentration is increased, substitution of H_2O ligands by Cl^- ions results in the formation of a number of Fe(III)-chloro complexes. At sufficiently high chloride concentration, Raman and EXAFS (extended X-ray absorption fine structure) studies indicate that the geometry of the complex changes from octahedral to tetrahedral (Apted et al., 1985; Murata et al., 1989). Spectrophotometric studies of ferrous chloride complexes indicate similar octahedral to tetrahedral transition at high salinity (Susak and Crerar, 1985; Zhao and Pan, 2001).

Most previous experiments report the formation constants of the $FeCl^{2+}$ and/or $FeCl_2^+$ complexes at ionic strength greater than zero, but there are significant discrepancies even at given ionic strengths (Moller, 1937; Rabinowitch and Stockmayer, 1942; Woods et al., 1962; Rowley and Sutin, 1970; Rao and Rao, 1971; Strahm et al., 1979; Byrne and Kester, 1981; Brubaker and Peterson, 1989; Inada and Funahashi, 1999). Another limitation of many pre-1980 studies is that they usually assumed that only one ferric chloride complex was present in the sample solution at a particular chloride concentration and ionic strength when fitting the experimental data. This ignored the possible co-existence of other complexes and probably affected the accuracy of the calculated equilibrium constants. Recently, Tagirov et al. (2000) reported standard state thermodynamic properties of $FeCl^{2+}$ from 25 to 90 °C measured using a non-isothermal electrochemical technique; however, no reliable and consistent thermodynamic properties for higher order chloro complexes, i.e., $FeCl_2^+$, $FeCl_{3(aq)}$ and $FeCl_4^-$ are available. A few studies have reported formation constants of $FeCl_2^+$ and $FeCl_{3(aq)}$, but they are in poor agreement. To the authors' knowledge only two studies provided equilibrium constants for aqueous $FeCl_4^-$ at 25 °C (Gamlen and Jordan, 1953; Marcus, 1960), although a Raman study by Murata et al. (1989) suggested that tetrahedral $FeCl_4^-$ predominates at 300 °C in solutions with chloride concentration greater than 3 m.

In the past two decades, geologists and geochemists have developed databases of thermodynamic properties of minerals and aqueous species, aimed at modelling chemical processes in geological systems, e.g., the Lawrence Livermore National Laboratory and UNITHERM databases (Wolery, 1992; Shvarov and Bastrakov, 1999, respectively). Due to the lack of thermodynamic data, these databases do not contain high temperature properties of $FeCl_{3(aq)}$ and $FeCl_4^-$, two complexes that are likely to be important in oxidised saline solutions at elevated temperature and pressures.

The study of metal speciation in hypersaline brines is difficult due to several theoretical and practical factors. On the one hand, activity–composition relationships for trace elements in hypersaline solutions are poorly understood (e.g., Helgeson and Kirkham, 1974), which renders the quantitative interpretation of the data difficult. On the other hand, most traditional experimental techniques are difficult to apply to these systems. For example, the high absorbance of x-rays by the salt makes X-ray absorption measurements more difficult, and high solubilities often limit the use of

solubility experiments to relatively low salt concentrations (e.g., Liu et al., 2001). In the case of Fe(III), it should be possible to measure the solubility of hematite up to high salinity, but previous hematite solubility experiments up to 200 °C are inconsistent probably due to non-equilibrium and/or formation of amorphous coatings (Tagirov et al., 2000). This paper aims to show that it is possible to obtain speciation models that are consistent with information obtained by various techniques despite our limited understanding of the thermodynamics of trace elements in hypersaline solutions. A better understanding of metal speciation in hypersaline brines resulting from this type of study will eventually serve as a basis for the further development of the theoretical understanding of trace metal speciation in brines. Specifically, this study explores the use of UV spectrophotometric and synchrotron XAFS experiments to identify important ferric chloride complexes forming over a wide range of chloride concentrations (up to 15 m) and temperatures (25–90 °C). Based on the experimental data generated from this and previous studies, a self-consistent set of thermodynamic properties for Fe(III) chloride complexes is presented, which can be used for modelling Fe speciation and transport in near-surface waters and oxidised hydrothermal systems.

This study involved an iterative process using all available experimental evidence to construct a consistent speciation model for Fe(III) chloride complexes in dilute and highly concentrated brines. In this report, we start by describing the UV–Vis spectrophotometric experiments and their interpretation, as this method provided the most complete insight into the nature and stability of Fe(III) chloride complexes. This model is then tested using X-ray Absorption Near Edge Structure (XANES) and EXAFS spectroscopy. EXAFS also provides further insight into the geometry of the Fe(III) chloride complexes.

2. Experimental

2.1. Sample solutions

The sample solutions for both UV–Vis spectrophotometry and XAFS experiments were prepared gravimetrically from $FeCl_3 \cdot 6H_2O$ (BDH AnalaR®), lithium chloride (SigmaUltra®) and doubly deionized water (Millipore Milli-Q). 0.1 m HCl was added to the solutions to minimise the hydrolysis of iron(III). In addition to the variable ionic strength measurements, the UV–Vis spectra of 14 solutions containing variable chloride concentrations (LiCl) but having a fixed ionic strength of 11.6 m maintained with Li-triflate ($LiCF_3SO_3$) were also measured. The Li traflate solutions were prepared with lithium hydroxide and distilled triflate acid. The total chloride and iron concentrations of the sample solutions used in the UV spectrophotometry and synchrotron XAFS measurements are listed in Tables 1 and 2, respectively.

2.2. UV–Vis spectrophotometry

Spectrophotometric measurements were carried out using a Varian CARY® 5G UV–Vis-NIR instrument equipped with a water-regulated temperature controller. The sample solutions were placed in 1-cm rectangular

Table 1
Composition of sample solutions used in the measurement of UV spectra

Fe (mm)	Cl total (m)	Li total (m)	HCl (m)	Triflate (m)
0.443	0.108	0.000	0.107	–
0.242	0.207	0.100	0.107	–
0.443	0.365	0.257	0.107	–
0.286	0.629	0.522	0.107	–
0.427	1.077	0.969	0.107	–
0.286	1.591	1.484	0.107	–
0.405	2.104	1.997	0.107	–
0.286	2.727	2.620	0.107	–
0.490	3.387	3.279	0.107	–
0.434	3.947	3.839	0.107	–
0.490	4.604	4.496	0.107	–
0.426	5.229	5.122	0.107	–
0.464	6.143	6.035	0.106	–
0.464	6.927	6.819	0.106	–
0.433	7.700	7.592	0.107	–
0.433	8.368	8.261	0.107	–
0.421	9.123	9.015	0.107	–
0.421	9.864	9.756	0.107	–
0.494	10.592	10.484	0.107	–
0.494	11.352	11.244	0.107	–
0.476	12.187	12.079	0.107	–
0.476	12.857	12.749	0.107	–
0.415	13.561	13.453	0.107	–
0.415	14.370	14.262	0.107	–
0.364	15.153	15.045	0.107	–
1.024	0.003	11.58	0	11.58
1.024	0.093	11.58	0.09	11.58
0.535	1.132	11.58	0.09	10.53
0.758	1.357	11.57	0.09	10.31
0.480	3.066	11.76	0.09	8.78
0.543	3.509	11.14	0.09	7.73
0.363	5.169	11.87	0.09	6.79
0.309	5.803	11.51	0.09	5.80
0.497	6.849	11.61	0.09	4.85
0.253	7.882	11.61	0.09	3.82
0.342	8.791	11.56	0.09	2.86
0.315	9.828	11.60	0.09	1.86
0.187	10.747	11.60	0.09	0.94
0.163	11.657	11.57	0.09	0.00

Table 2
Composition of sample solutions used in XAFS experiments (all solutions were acidified with 0.1 m HCl)

Solution no.	T (°C)	Fe_{tot} (m)	Cl_{tot} (m)	Li_{tot} (m)
2 mli	90	0.35	3.33	2.18
8 mli	90	0.34	8.34	7.22
15 mli	90	0.36	14.38	13.2
0 m	25	0.035	0.21	0
2 m	25	0.033	2.47	2.27
5 m	25	0.033	5.53	5.33
10 m	25	0.033	12.30	12.1
15 m	25	0.043	15.23	15.0

quartz cells sealed with a Teflon plug. For each solution, the spectrum of a Fe-free blank solution containing the same concentration of LiCl and HCl was collected before measuring the Fe-bearing solution. The baseline spectra were subtracted from the spectra of the sample solutions to correct for detector response and for absorption of the cell and LiCl solutions. Absorbances were measured at a 1-nm increment between 200 and 500 nm, and the absorbance range was typically between 0 and 2.5 absorbance units. Spectra were collected at temperatures of 25, 60 and 90 °C during the heating cycle. For most solutions, spectra were also collected during cooling. The difference between these spectra was generally less than 0.002–0.005 absorbance units, i.e., 0.2–0.5% when the absorbance unit is one, which is within error of our analytical precision. This indicates that there was no significant change in dissolved Fe(III) concentration (e.g. due to a leak or to precipitation of Fe-mineral) during heating and cooling cycles.

2.3. XANES and EXAFS

Iron K-edge (7112 eV) XANES and EXAFS spectra of Fe(III) in acidic chloride solutions containing up to 15 m LiCl were measured at 25 °C and 90 °C using the beamline BL-20B (Australian National Beamline Facility, ANBF) at the Photon Factory, Japan. BL-20B is a bending magnet beam-line equipped with a water-cooled channel cut Si(111) monochromator, has a horizontal acceptance angle of 2 mrad, and an energy resolution ($E/\Delta E$) of 2400. The beam size used was 2×1 mm^2. The incident beam intensity I_0 was measured with an ionisation chamber using a N_2 fill gas at atmospheric pressure. Data were measured in fluorescence mode with a Canberra GL0110S 10 element array Ge solid-state detector and collected from 6900 to 7897 eV, using 10 eV steps from 6890 to 7090 eV; 0.25 eV steps from 7090 to 7150 eV, and an increasing E step of 0.05–5.3 eV from 7150–7895 eV. The energy scale was calibrated using the $1s\rightarrow3d$ (pre-edge) peak, which is located at 7113.5(1) eV in Fe(III) compounds (Waychunas et al., 1986).

For measurements at 25 °C, the freshly prepared solution was placed into a Teflon solution cell equipped with Kapton windows. The cell to detector distance was varied with changing solution concentration, such that the total count measured at detector element 6 (one of the most central detector elements) remained at a relatively constant 60,000 counts per second. At 90 °C, a hydrothermal cell made from titanium (grade 2) and equipped with Kapton windows was used. The cell was placed in a cylindrical aluminum block hosting two cartridge heaters. The temperature was controlled by a solid-state temperature controller to a precision of ±1 °C.

3. Interpretation of UV–Vis spectrophotometric experiments

Solution UV–Vis-NIR spectrophotometry measures the electronic transitions between orbitals of soluble molecules and ions and therefore provides information about the electronic structure of the complex, e.g., the oxidation state of the metal, the geometry of the complex, and the nature of the ligands. The intensity of electronic transitions (molar absorbance) occurring in the 200–500 nm region for the Fe(III)-chloride system indicates that the bands originate from ligand to metal (L→Fe(III)) charge transfer transitions, although in the higher energy UV region there may also be contributions from charge transfer transitions to the solvent.

The quantitative interpretation of UV–Vis spectra is based on the Beer-Lambert law, which relates the absorbance (A) at a given wavelength (λ) to the molar absorptivities ($\varepsilon_{i,\lambda}$) and the molar concentrations (M_i) of each of the i absorbing species present in solution:

$$A_\lambda = l\sum_{i=1}^{n} M_i\varepsilon_{i,\lambda}, \quad (1)$$

where n is the number of the absorbing species and l is the path length of the cell. Deviations from the Beer-Lambert law at high salinity are expected due to the influence of the dielectric constant (or refractive index) of the medium on the absorption of light by a particular complex (Clifford and Crawford, 1966). This effect produces a 4% increase in molar absorptivity for a species in pure H_2O and in 10 m LiCl at 589 nm (data from Lide, 2003). Deviations from the Beer-Lambert law are also

expected because changes in the electronic structure of the complex can be induced by changes in the structure of the solvent and in the outer coordination shells of the complex (i.e., variations in ion association). For example, a contraction of the coordination shell by 0.1 Å is observed for the hydrated Ag^+ ion as temperature increases from 25 °C to 350 °C (Seward et al., 1996). These complex effects are difficult to quantify, but indirect evidence suggest that these effects are small for the Fe(III)-chloride system under investigation. Firstly, $FeCl_4^{2-}$ is the predominant and only Fe(II) species present above ~12 m LiCl at 100 °C (Zhao and Pan, 2001). Hence, the UV–Vis spectrum of Fe(II)-chloride solutions is not expected to change at salinities above 12 m if the Beer-Lambert law is strictly valid. Zhao and Pan (2001) observed a small but significant change of ±2% in the molar absorptivity coefficient of the solution over the peak at 37,500 cm^{-1}. The reported variation appears to vary in a non-linear fashion with salt concentration. Secondly, Bjerrum et al. (1975) note that the spectra for $CoCl_4^{2-}$ are very similar (within 2%) in LiCl and HCl solutions, despite the different compositions of the solutions, which is very likely to cause variations in ionic association.

Experiments conducted at fixed ionic strength are commonly used to study speciation in concentrated electrolyte solutions, following the assumption that activity coefficients are dependant upon the ionic strength only. This type of experiment does not remove the fundamental physical problems (such as the effects of refractive index, structure of the solvent and ion association on the validity of Beer-Lambert law) and they introduce complications in ion association, e.g., $Li^+...Cl^-$ vs. $Li^+...O_3SCF_3^-$. These variations in ionic association will lead to changes in the activity of the ions present. As a consequence, ion pairing between anionic species and even neutral species (e.g., $FeCl_4^-$ and $FeCl_{3(aq)}$ of interest here) and Li^+ will be affected and the variations in the relative concentration of the two anions, Cl^- and $CF_3SO_3^-$ will affect interactions between these anions and cationic Fe–Cl species (e.g., $FeCl^{2+}$ and $FeCl_2^+$). These factors can influence the spectrum of the species present in solution.

The variable ionic strength experiments favoured here have the advantage of leading to thermodynamic properties for Fe(III)–Cl complexes that are consistent with the results obtained at low ionic strength while allowing the estimation of the solution compositions at high salt concentration. The properties can be used in most common geochemical modelling packages with no or little modification. Such thermodynamic properties are difficult to obtain from single ionic strength data. A set of experiments conducted at a fixed ionic strength of 11.6 m show that the speciation is qualitatively similar under conditions of varying and fixed ionic strengths.

Hence, for the quantitative interpretation, we use the varying ionic strength experiments and assume that deviations from Beer-Lambert law at high salinity can be neglected in the case of the Fe(III)-chloro complexes under investigation. This means we assume that over the range of predominance of a particular complex, the Beer-Lambert law is obeyed, or at least the variation in absorbance of the complex with concentration at a particular wavelength is near-linear with salt concentration. The analysis would therefore return the average spectrum for the species. The quantitative analysis conducted here includes strong constraints regarding variation of species concentration with increasing salt concentration (mass action and mass balance constraints; see below). Hence, this analysis will treat non-linear deviations from the Beer-Lambert law as noise. Special care, however, should be taken for the interpretation of speciation change at very high salinity, where changes to the last predominant species may not represent a new species.

Ultimately, the consistency of the speciation models derived from the UV–Vis experiments (both under varying and fixed ionic strength) with the results of the XANES and EXAFS experiments offers the strongest evidence about the validity of this approach. The thermodynamic analysis used has the advantage to be fully consistent with the common approach used for the low salinity part of the system (< 1 m). Thermodynamic properties presented here for the species present at high salinity are dependant upon the choice of the thermodynamic model and should be considered as apparent properties. However, in the absence of well-established theory about activity–composition relationships for trace elements in highly concentrated electrolytes, this empirical approach is justified. It should also be emphasised that this simple approach does indeed succeed in reproducing the experimentally observed speciation changes.

3.1. Qualitative interpretation

The molar absorptivities (absorbance divided by total iron molar concentration) of ferric chloride measured at 25, 60 and 90 °C for solutions containing between 0.1 and 15 m LiCl are shown in Fig. 1. The spectra collected at 25 °C are similar to those recorded in previous studies under similar conditions (e.g., Friedman, 1952; Gamlen and Jordan, 1953; Byrne and Kester, 1981), but the data

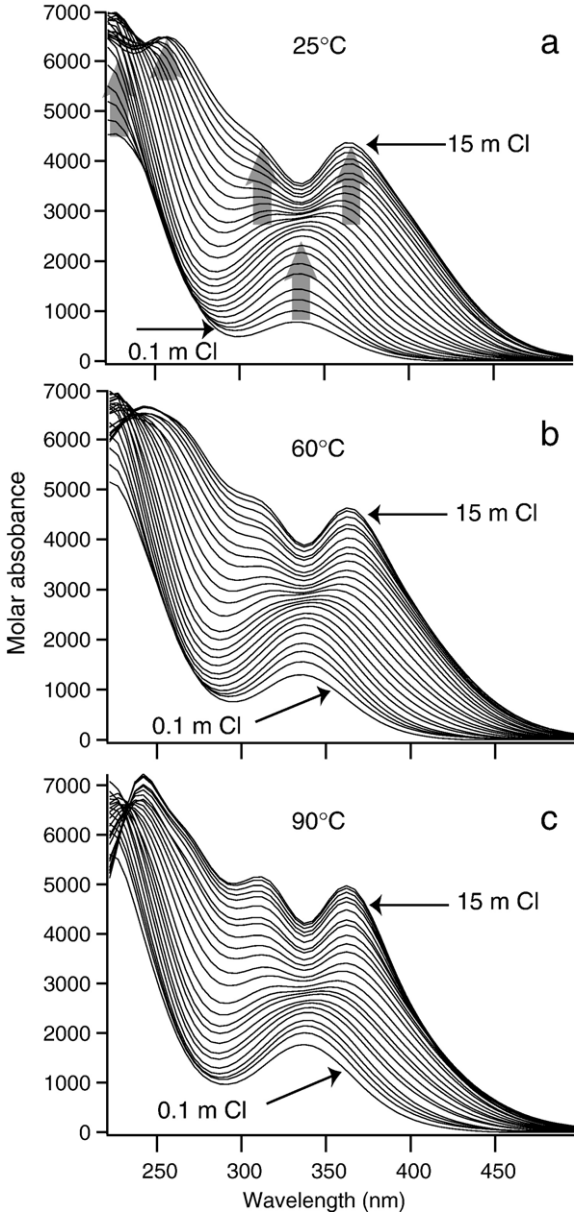

Fig. 1. Molar absorptivity of ferric chloride complexes in 0.1–15 molal LiCl solutions containing 0.1 M HCl at 25 °C (a), 60 °C (b) and 90 °C (c). The grey arrows indicate the absorption peaks of the Fe(III)-chloro complexes.

presented here cover a much wider range of chloride concentrations. The maxima at 335 nm and below 250 nm that appear in the 1–5 m LiCl concentration range were attributed to the formation of $FeCl_2^+$, with a minor contribution from $FeCl^{2+}$. Increasing the chloride concentration above 5 m results in the growth of a new peak at 365 nm and of a shoulder at 310 nm. When the chloride concentration exceeds 10 m, the peak at 365 nm becomes significant and a new peak appears at around 260 nm, and the intensity of the peaks at 250 and 335 nm decreases (Fig. 1).

These changes are attributed to the absorption by $FeCl_{3(aq)}$ and $FeCl_4^-$ (Friedman, 1952; Gamlen and Jordan, 1953), and reflect the change in the geometry of the complex. The spectra collected at 60 °C and 90 °C are similar to the 25 °C spectra, but it is clear that with increasing temperature, the bands at 365 and 260 nm due to $FeCl_{3(aq)}$ and $FeCl_4^-$ become more significant, and the shoulder at 310 nm at 25 °C becomes a clear peak at 90 °C. These features indicate qualitatively that the high order $FeCl_{3(aq)}$ and $FeCl_4^-$ complexes become more stable with increasing temperature.

3.2. Principles of quantitative interpretation

The procedure used to fit the spectra is similar to the method established by Brugger et al. (2001) for UV–Vis spectrophotometric experiments on Cu(II) chloride complexes. This method was also used in the study of Cu(I) chloride speciation (Liu et al., 2002). Since the fitting procedures are described in detail in these two publications, only a brief summary is given here.

The Beer-Lambert law is based on the molar concentration scale, and a molar to molal conversion factor f_s is required when using the molal scale (e.g., Heinrich and Seward, 1990):

$$A_\lambda = \frac{1}{f_s} l \sum_{i=1}^{n} M_i \varepsilon_{i,\lambda}, \text{ where } f_s = \frac{1000 + W_{\mathrm{LiCl}} m_{\mathrm{LiCl}}}{1000 \rho_{LiCl(m_{\mathrm{LiCl}},T)}}, \quad (2)$$

W_{LiCl} is the molecular mass of LiCl, m_{LiCl} is the total molality of LiCl in the solution, and $\rho_{\mathrm{LiCl}(m_{\mathrm{LiCl}},T)}$ is the density (g/m^3) of LiCl solutions at temperature T in Kelvin. The density of the LiCl solution is calculated using the power function presented by Brugger et al. (2001), which used least squares methods to fit various experimental density data of LiCl solutions. The density of LiCl-Li-triflate solutions is estimated volumetrically (J. Black, unpublished data).

When considering more than one wavelength, the Beer-Lambert law (Eq. (1)) can be written in a matrix form as:

$$\mathbf{A} = \mathbf{C}^*\mathbf{E} \quad (3)$$

where $\mathbf{A}$ is the matrix of measured absorbance (number of solutions × number of wavelengths), $\mathbf{C}$ is

the matrix of concentration of absorbing species (number of solutions × number of absorbing species) and **E** is the matrix of molar absorptivity for all absorbing species (number of absorbing species × number of wavelengths). The goal of data analysis is to find the matrices **C** and **E** that best reproduce the observed absorbance spectra, i.e., matrix **A**, by optimising both formation constants and molar absorptivities for each absorbing ferric chloride complex. Practically, this simple linear algebra problem has an infinite number of solutions, whereas there is only one physical solution. This unique solution can be retrieved by introducing physical constraints (e.g., concentrations and molar absorptivities are positive numbers; chemical mass action and mass balance) into the model. This usually renders the problem non-linear, and non-linear least-square techniques are required to retrieve **E** and **C**.

In this paper, the following procedure was used to analyse the spectrophotometric data. First, principal component analysis (e.g., Malinowski and Howery, 1980) was applied to estimate the minimum number of absorbing species necessary to explain the experimental dataset (Brugger et al., 2001; Liu et al., 2002). A preliminary data analysis, aimed at obtaining some information about the number and nature of the Fe(III) chloride complexes present in the experiments, was conducted using "model-free" analysis (De Juan et al., 1997). This approach implements non-negativity constraints for molar absorptivity coefficients and concentrations (i.e., $\varepsilon_\lambda \geq 0$ and $c_i \geq 0$) as well as mass balance for Fe(III), and allows the concentration profiles and molar absorptivity coefficients for the absorbing species to be determined without the need to make assumptions about the chemistry of the system beyond the number of absorbing species present. On the basis of this preliminary analysis and taking into account available literature information, a speciation and a thermodynamic model were established. The final quantitative analysis is conducted using non-negativity constraints for the molar absorptivity coefficients, and a complete speciation model to calculate the matrix **C** (i.e., the elements of **C** are constrained by mass balance and mass action equations). This analysis delivers a set of equilibrium constants (log$K$) for the formation of the different Fe (III)-chloride complexes. The uncertainties in the log$K$ values were then evaluated using maps of the residual function. Spectral data measured between 240 and 500 nm for all 25 sample solutions at 25, 60 and 90 °C with chloride concentrations of 0.1–15 m were used in the analysis.

3.3. Principal Component Analysis (PCA)

The residual function (R) used in PCA is defined as:

$$R = 100\sqrt{\frac{\sum(x_i - x)^2}{\sum x_i^2}} \quad (4)$$

where x_i and x are the measured and calculated absorbance values, respectively. PCA of the spectra collected at each temperature indicates that for all three series of spectra at least 5 factors are required to describe the spectra within an analytical precision of 0.2–0.5% (Fig. 2). This 5th factor also corresponds to a break in the slope of the residual curve in Fig. 2, which indicates a change in the physical significance of each factor. The first 5 factors are interpreted to represent five absorbing Fe(III) chloride complexes (e.g., Fe^{3+}, $FeCl^{2+}$, $FeCl_2^+$, $FeCl_{3(aq)}$ and $FeCl_4^-$), while the additional factors account for experimental noise and/or deviations from

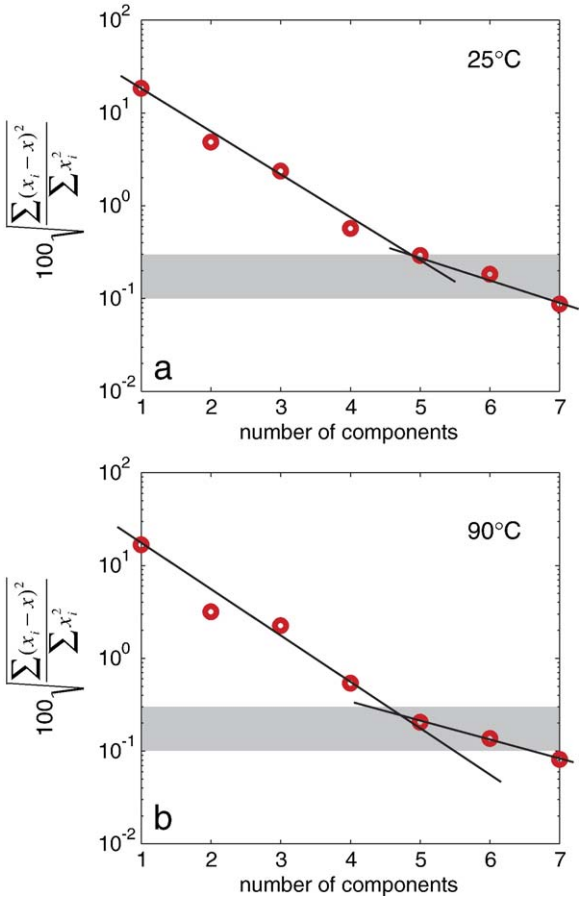

Fig. 2. Principal component analysis on spectrophotometric data at 25 °C and 90 °C. The circles represent calculated residuals corresponding to the number of factors on the x axis. The grey area indicates the level of analytical uncertainty of 0.2–0.5%.

the linear Beer-Lambert law. If the noise was perfectly random, each additional factor would result only in a small decrease in residuals (e.g., Meloun et al., 2000); for real data, however, noise is not random, and even in simple systems with pure variables (i.e., wavelength at which only one species absorbs) a significant correlation exists (e.g., Fig. 5 in Meloun et al., 2000).

3.4. "Model-free" interpretation and choice of speciation model

Note that for the reason of simplicity, all Fe(III) chloride complexes are written without water molecules throughout the paper, unless the geometry of the complex needs to be emphasised. Species (1) corresponds to the hexaaquo complex, $Fe(H_2O)_6^{3+}$ (e.g., Byrne and Kester, 1981). The next species (2) is dominant at chloride concentrations between 0.3 and 4 m. Previous studies agreed that $FeCl^{2+}$ (i.e., octahedral $[FeCl(H_2O)_5]^{2+}$) is dominant in low chloride concentration solutions, so species (2) probably corresponds to this species. The following species (3) has a molar absorbance spectrum similar to $FeCl_2^+$ and hence corresponds to $FeCl_2^+$ (octahedral $[FeCl_2(H_2O)_4]^+$; e.g., Gamlen and Jordan, 1953; Marcus, 1960; Byrne and Kester, 1981; Tagirov et al., 2000). The next two species have spectra that differ from those of the octahedral $FeCl^{2+}$ and $FeCl_2^+$, and are attributed to $FeCl_{3(aq)}$ and $FeCl_4^-$. $FeCl_4^-$ is usually assumed to be the highest limiting Fe(III) chloride complex (e.g., Friedman, 1952; Gamlen and Jordan, 1953), so species (5) is proposed to be this complex. The tetrahedral $[FeCl_4^-]$ ion is very stable; for example, among the 90 compounds listed by Melnik et al. (1997) as containing Fe(III) in 4-fold coordination, 66 contain the $FeCl_4^-$ complex. Hence, there is little doubt that $FeCl_4^-$ in hypersaline solution exits with tetrahedral geometry. $FeCl_{3(aq)}$, on the other hand, may exist as tetrahedral $[FeCl_3(H_2O)]_{(aq)}$ or as trigonal bipyramidal $[FeCl_3(H_2O)_2]_{(aq)}$. The latter geometry was favoured by Kubicki (2001) for the $[Fe(OH)_2(H_2O)_3]^+$ complex on the basis of quantum mechanical calculations.

Hence, the following five complexes were included in the speciation model: Fe^{3+}, $FeCl^{2+}$, $FeCl_2^+$, $FeCl_{3(aq)}$ and $FeCl_4^-$. In most solutions $FeCl^{2+}$ is present in low concentrations, and its formation constant cannot be accurately obtained from our experiments, but it is still necessary to include this species in the speciation model as it has a significant contribution to the spectra of solutions with low chloride concentration. Therefore, the log$K$ values of this species were taken from the thorough study by Tagirov et al. (2000); these values are also in good agreement with the earlier room-temperature studies of Rabinowitch and Stockmayer (1942) and Bray and Hershey (1934). log$K$ values for the other three complexes ($FeCl_2^+$, $FeCl_{3(aq)}$ and $FeCl_4^-$) were determined from our experimental data. Polynuclear Fe(III) species such as $[Cl_3Fe–O–FeCl_3]^{2-}$ (e.g., Solbrig et al., 1982) are unlikely to be present at the low Fe concentrations used in the UV–Vis experiments, and were ignored. Even under the acidic conditions (0.1 m HCl) used in these experiments one needs to check for the possibility of deprotonation of the water coordinated to Fe(III), as the pK for the reaction $Fe^{3+}+H_2O=Fe(OH)^{2+}+H^+$ at 25 °C is around 2.19 (Baes and Mesmer, 1976; the available experimental results are close to this value, e.g., 2.18 from Zotov and Kotova, 1979; 2.20 from Millero et al., 1995; and 2.18 from Byrne et al., 2000) and decreases to 0.83 at 90 °C (interpolated from Zotov and Kotova, 1980). Speciation calculations show that $FeOH^{2+}$ only account for less than 5% of the Fe in the lowest chloride concentration solutions, and less than 0.1% at 2 m Cl concentration at 90 °C. Moreover, $Fe(OH)^{2+}$ displays an absorbtion band at ~305 nm (Zotov and Kotova, 1979), which is absent from our spectra. Because the data analysis only fits formation constants for complexes that become dominant about 2 m chloride concentration, $Fe(OH)^{2+}$ was not incorporated in the final speciation model.

The full dataset (0.1–15 m LiCl) was used for the "model-free" analysis. Using 5 factors, the smooth succession of species expected for step-wise replacement of H_2O ligands by chloride ions was obtained (Fig. 3a). When 6 factors were used, however, none of the possible models converged. In general, the concentration of the 6th factor was found to vary in parallel to that of the 5th factor, while the molar absorptivity of both species were highly correlated. This strongly suggests that a 6th factor was not necessary to interpret the data; the 6th factor may for example be related to deviations from the Beer-Lambert Law at high salinity rather than to a change in metal speciation.

3.5. Experiments at fixed ionic strength of 11.6 m

The spectra of Fe(III)-chloro-complexes measured at fixed ionic strength of 11.6 m with LiCl-Li-triflate solutions are similar to those measured in LiCl solutions at varying ionic strength (Figs. 4 and 1, respectively). The major difference is that the high ionic strength medium appears to stabilise the non-octahedral species. For example, the peak at ~310 nm, which is characteristic of the $FeCl_{3(aq)}$ species (Fig. 3b), is well resolved at chloride concentrations above ~9 m in the

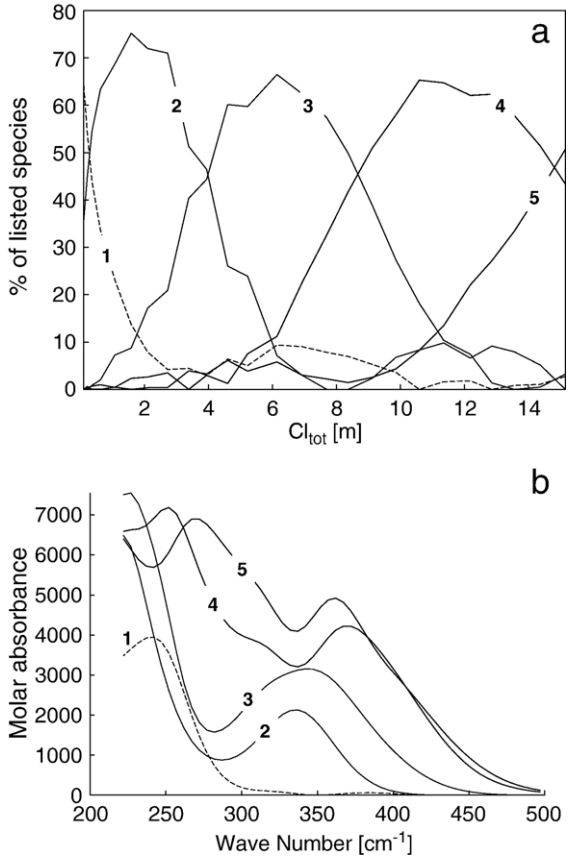

Fig. 3. Results from the "model-free" analysis. (a) Distribution of absorbing species. (b) Molar absorbance spectra for the 5 species.

varying ionic strength experiments, and at 0.6 m in the fixed ionic strength experiment. PCA analysis further provides support for the similarity of Fe(III) speciation in both sets of experiments (Figs. 4b and 2a), five species being required to explain the datasets within analytical uncertainty. Note that for the high ionic strength experiments at 90 °C, spectra were collected only for Cl concentrations above 0.6 m; this results in the loss of one factor (corresponding to Fe^{3+}) in the PCA analysis (Fig 4d). Attempts to apply model-free analysis to the fixed ionic strength dataset were not successful; the system was found to be mathematically unstable, and often converged to unrealistic solutions (e.g., negligible concentrations for one species correlated with extremely large molar absorptivity coefficients). This is probably due to the fact that more spectra are required to constrain the low salinity part of the dataset. However, this does not affect the major results obtained for the fixed ionic strength experiment, namely that the speciation of Fe is very similar in the different electrolytes (LiCl at varying ionic strength; LiCl–Li-triflate under fixed ionic strength), and the main difference is a higher stability of the non-octahedral complexes at high ionic strength; this is to be expected because the lower H_2O content of these complexes correlates with the lower activity of H_2O in the high ionic strength solutions.

3.6. The thermodynamic model

The following aqueous species are included in the model: H^+, Li^+, Cl^-, $LiCl_{(aq)}$, $HCl_{(aq)}$, Fe^{3+} and four Fe(III) chloride complexes. The concentrations and activities of aqueous species were calculated by solving simultaneously the following mass action equations, mass balance equations, and a charge balance equation:

$$K_{HCl_{(aq)}} = \frac{m_{HCl_{(aq)}}\overline{\gamma}_{HCl_{(aq)}}}{m_{H^+}m_{Cl^-}\overline{\gamma}_{H^+}\overline{\gamma}_{Cl^-}}, \quad (5)$$

$$K_{LiCl_{(aq)}} = \frac{m_{LiCl_{(aq)}}\overline{\gamma}_{LiCl_{(aq)}}}{m_{Li^+}m_{Cl^-}\overline{\gamma}_{Li^+}\overline{\gamma}_{Cl^-}}, \quad (6)$$

$$K_{FeCl_i^{3-i}} = \frac{m_{FeCl_i^{3-i}}\overline{\gamma}_{FeCl_i^{3-i}}}{m_{Fe^{3+}}\overline{\gamma}_{Fe^{3+}}\left(m_{Cl^-}\overline{\gamma}_{Cl^-}\right)^i}, \quad (7)$$

$$m_{Fe_{total}} = \sum_i m_{FeCl_i^{3-i}}, \quad (8)$$

$$m_{Cl_{total}} = m_{HCl_{(aq)}} + m_{LiCl_{(aq)}} + m_{Cl^-} + \sum_i i m_{FeCl_i^{3-i}}, \quad (9)$$

$$m_{Li_{total}} = m_{LiCl_{(aq)}} + m_{Li^+}, \quad (10)$$

$$m_{Li^+} + \sum_i (3-i) m_{FeCl_i^{3-i}} = m_{Cl^-}, \quad (11)$$

where K, m and $\overline{\gamma}$ refer to the formation constants, molal concentration and activity coefficient for the subscripted individual species, respectively, and i in Eqs. (7)–(9), and (11) refers to the number of chloride ligands. Following Brugger et al. (2001) and Liu et al. (2002), an extended form of the Debye-Hückel equation was used:

$$\log(\overline{\gamma}n) = -\frac{A_\gamma Z_n^2 \overline{I}^{1/2}}{1 + B_\gamma \mathring{a}_n \overline{I}^{1/2}} + b_{\gamma,LiCl}\overline{I} + b_{\gamma_{sq},LiCl}\overline{I}^2 + \Gamma_\gamma, \quad (12)$$

where A_γ and B_γ are the Debye-Hückel solvent parameters taken from Helgeson and Kirkham (1974), and $b_{\gamma,LiCl}$ is the extended-term parameter (b-dot

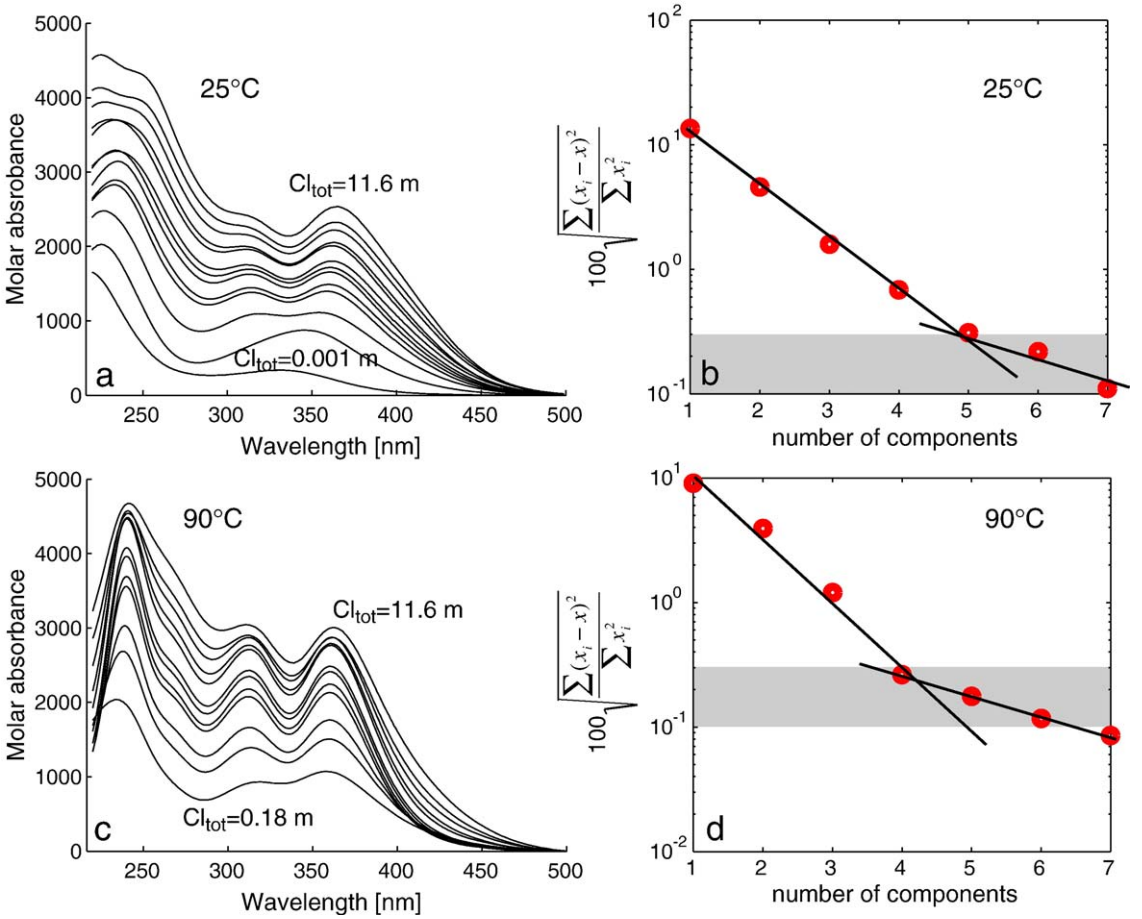

Fig. 4. Molar absorptivity of ferric chloride ion LiCl–Li-triflate solutions with ionic strength of 11.6 m, at 25 °C (a) and 90 °C (c). The corresponding principal component analysis is shown in (b) and (d), respectively.

coefficient) for LiCl-dominated solutions, $\mathring{a}_n$ is the distance of closest approach of ion n, and is given a value of 5 Å for divalent and trivalent ions, and 4.0 Å for monovalent ions, except for H^+ and Fe^{3+} which are given a value of 9 Å (Kielland, 1937). $\bar{I}$ is the effective ionic strength using the molal scale. Γ_γ is a mole fraction to molality conversion factor and $b_{\gamma_{sq},LiCl}$ is a quadratic term added to the Debye-Hückel equation to extend its validity to high chloride concentrations (up to 18 m LiCl; Brugger et al., 2001). This approach allows us to describe more accurately the experimental mean molal stoichiometric activity coefficient data for LiCl solutions (i.e., Holmes and Mesmer, 1983), and yields internally consistent activity coefficients for the Fe(III) chloride complexes. The activity coefficient of the neutral species, $LiCl_{(aq)}$, was estimated with the Setchénow equation (Setchénow, 1889; see Brugger et al., 2001):

$$\log(\bar{\gamma}_{LiCl_{(aq)}}) = b_{\gamma,LiCl_{(aq)}}\bar{I} + \Gamma_\gamma. \quad (13)$$

Values of the b-dot coefficient ($b_{\gamma,LiCl}$), Setchénow coefficient ($b_{\gamma,LiCl_{(aq)}}$) and the extended quadratic coefficient ($b_{\gamma_{sq},LiCl}$), at each experimental temperature were taken from Brugger et al. (2001). Formation constants for $HCl_{(aq)}$ and $LiCl_{(aq)}$ were from SUPCRT database (Johnson et al., 1992), and for $FeCl^{2+}$ from Tagirov et al. (2000). The activity coefficient for $HCl_{(aq)}$ was assumed to be unity. This is not expected to have an effect on the calculated parameters as it is only a minor species in the solutions and since there are no pH dependent equilibria pH values were not required in our data interpretation. Another neutral species, $FeCl_{3(aq)}$, however, is an important species in our experimental solutions, but since the Setchénow coefficient for this complex is unknown, a value of 0.1 was chosen as in previous studies by Brugger et al. (2001). The effect of this choice on the final speciation model and $\log K_{FeCl_{3(aq)}}$ is discussed below.

3.7. Quantitative analysis and estimation of uncertainties

Table 3 and Fig. 5 show the formation constants of Fe(III) chloride complexes at 25, 60 and 90 °C generated from the experimental data using the procedure described above. Fig. 5 indicates that while the formation constants for all three complexes increase with increasing temperature, the trend for $FeCl_{3(aq)}$ and $FeCl_4^-$ is steeper than $FeCl_2^+$, indicating that these two complexes become relatively more important with increasing temperature.

The uncertainties in the experimentally derived log$K$ values arise from many sources, such as error in solution concentration, instrument accuracy and parameters used in the calculation of activity coefficients and speciation. The derived log$K$ values are sensitive to the model used for calculating activity coefficients. For example, a change of the Setchénow coefficient of $FeCl_{3(aq)}$ by a factor 2 changes $\log K_{FeCl_{3(aq)}}$ by about 0.4 log units. In this study the uncertainties were estimated using a similar approach to that applied by Liu et al. (2002, 2001). This treatment of errors assesses only model-independent uncertainties arising from analytical errors and the non-fully constrained nature of the problem. The difference between the experimental spectra and the spectra calculated as a function of equilibrium constant for the formation the of Fe(III) chloride complexes $FeCl_2^+$, $FeCl_{3(aq)}$ and $FeCl_4^-$ was used to examine the nature of the minimum in the residual function and to estimate the magnitude of the uncertainties in the derived log$K$ values. The 2-dimensional sections through the 3-dimensional residual space are shown in Fig. 6 for experiments at 25, 60 and 90 °C. It is clear that there is a single minimum at each of the three temperatures, implying that all three complexes were present in detectable concentrations and their log$K$ values can be determined statistically. The statistical method of Draper and Smith (1998, p. 516) was used to define an approximate confidence region to estimate the uncertainties in log$K$ values at the 90% confidence level. For example, at 25 °C, the 90% confidence region is defined by the contour at 0.926% of the value of the absolute minimum, leading to uncertainties of ±0.25 for $FeCl_2^+$ and $FeCl_{3(aq)}$, and ±0.45 for $FeCl_4^-$ (Fig. 6a and b). The uncertainties for the other temperatures listed in Table 3 were estimated in the same way (Fig. 6).

Table 3
Logarithms of formation constants for Fe(III) chloride complexes derived from the UV spectrophotometric data

Reaction	25 °C	60 °C	90 °C
$Fe^{3+}+2Cl^-=FeCl_2^+$	+1.87±0.25	2.52±0.4	3.38±0.3
$Fe^{3+}+3Cl^-=FeCl_{3(aq)}$	0.77±0.25	1.55±0.3	2.75±0.3
$Fe^{3+}+4Cl^-=FeCl_4^-$	−1.26±0.45	−0.38±0.55	0.96±0.45

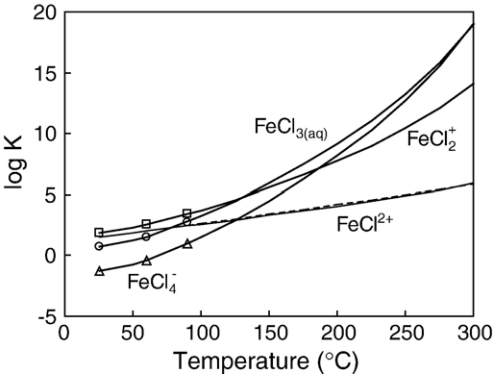

Fig. 5. Formation constants for $FeCl^{2+}$, $FeCl_2^+$, $FeCl_{3(aq)}$ and $FeCl_4^-$ complexes. The symbols show the experimental data from this study, the solid lines represent extrapolated values using the density equation of Anderson et al. (1991), and the dashed line shows Tagirov et al.'s (2000) extrapolation.

3.8. Calculated molar absorptivity spectra and speciation

Fig. 7 shows calculated molar absorptivities for four absorbing Fe(III) chloride complexes ($FeCl^{2+}$, $FeCl_2^+$, $FeCl_{3(aq)}$ and $FeCl_4^-$). At room temperature, the shape of the calculated molar absorbance peaks of Fe^{3+} (240–250 nm) and $FeCl^{2+}$ (335–340 nm) are very similar to that from previous studies. Note that the two small shoulders at 300 and 380 nm in the retrieved spectra of Fe^{3+} at 60 and 90 °C are caused by numerical uncertainty resulting from the very small concentration of this species in most solutions. The molar absorptivity spectra of $FeCl_2^+$ and $FeCl_{3(aq)}$ are also similar to those reported in Byrne and Kester (1981) and Gamlen and Jordan (1953). The molar absorptivity spectra of $FeCl_4^-$ are similar to those reported by Gamlen and Jordan (1953) and to the spectra of $KFeCl_4$ in ethylene bromide and in diethyl ether measured by Friedman (1952).

The spectra of $FeCl^{2+}$ and $FeCl_2^+$ have similar shapes, with $FeCl_2^+$ being characterised by higher molar absorptivity and a red shift of ~5 nm at 25 °C and 50 nm at 90 °C. This is characteristic for the replacement of one H_2O ligand by a chloride in octahedral species. The spectrum of $FeCl_{3(aq)}$, does not follow this trend, and is similar to that of tetrahedral $FeCl_4^-$. This suggests that $FeCl_{3(aq)}$ exists at least partly

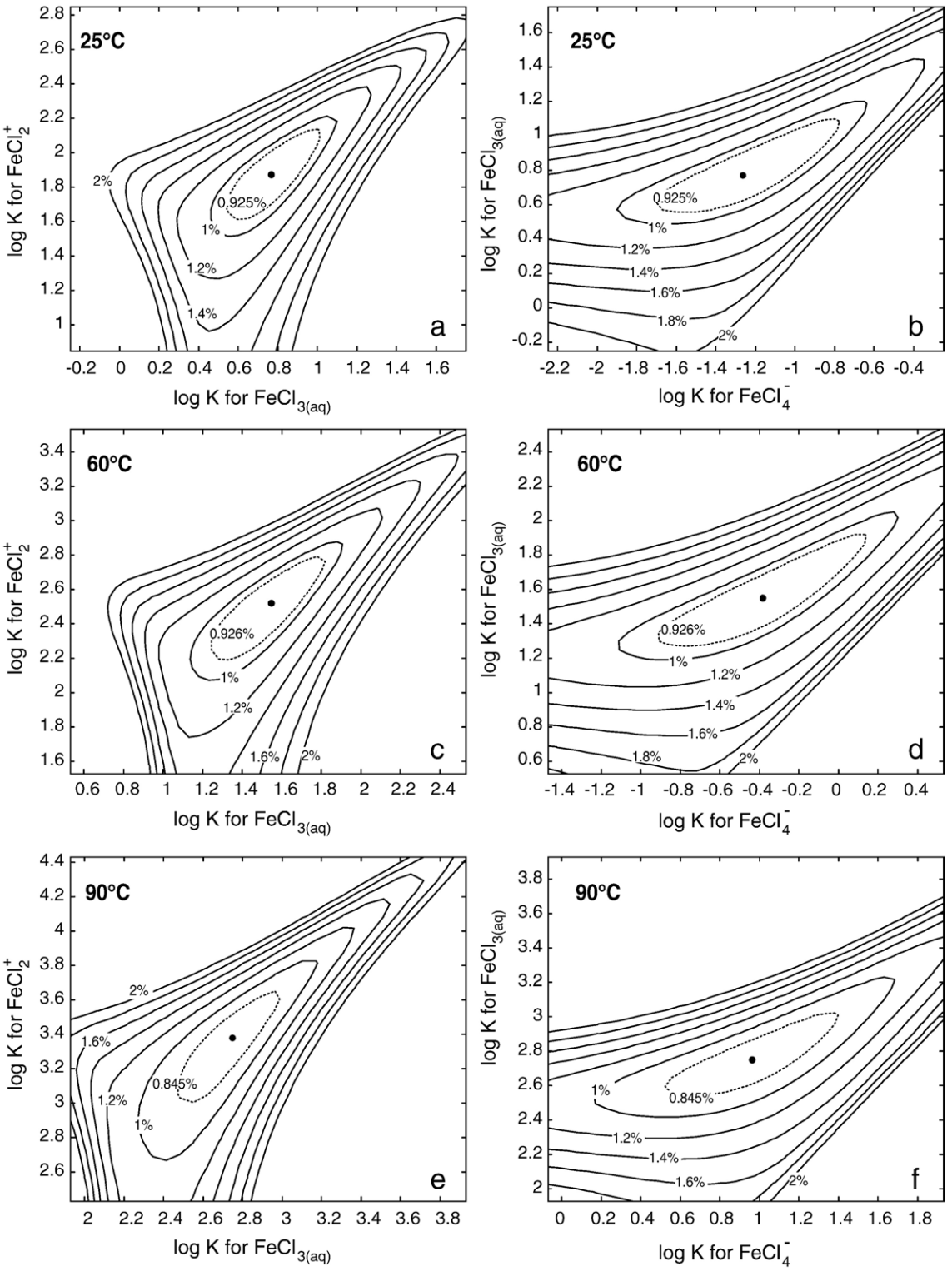

Fig. 6. Maps of the residuals from fitting of spectral data. The solid contours represent residual (R) in percentage as a function of log$K$ values for Fe (III) chloride complexes labelled in axis title. The dashed line stands for a 90% confidence region, and the black dots are fitted log$K$ values.

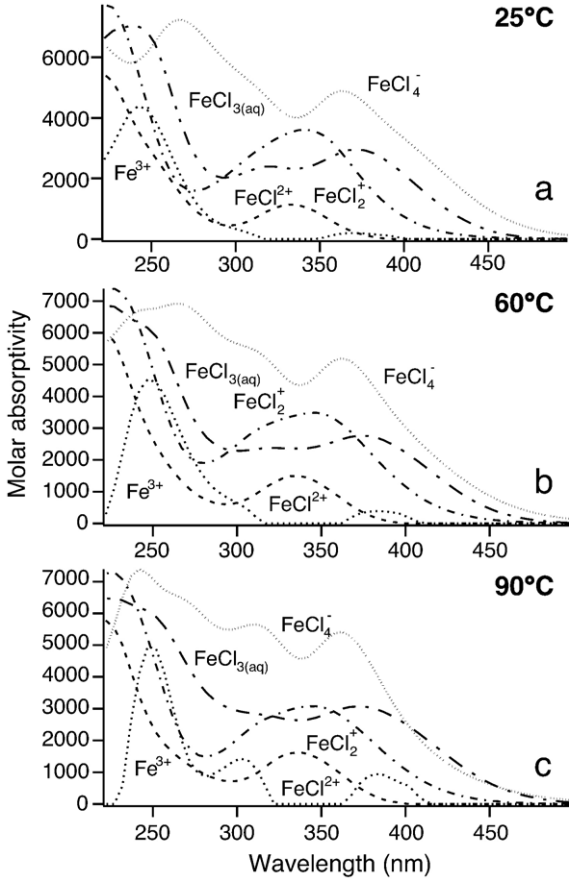

Fig. 7. Molar absorptivity spectra for individual Fe(III) species obtained from the analysis of UV–Vis spectrophotometric data at 25, 60 and 90 °C.

as a non-octahedral species, i.e., $[FeCl_3(OH_2)]_{(aq)}$ or, possibly, trigonal dipyramidal $[FeCl_3(OH_2)_2]_{(aq)}$. The spectra of $FeCl^{2+}$, $FeCl_2^+$ and $FeCl_{3(aq)}$ show little qualitative variation with increasing temperature. However, the spectrum of $FeCl_4^-$ shows an increase in the band at ~310 nm. This suggests an as yet unknown change in the electronic structure of the complex with increasing temperature.

Fig. 8 shows the calculated distribution of Fe(III) chloride complexes in the experimental solutions. It can be seen that $FeCl^{2+}$ dominates in low chloride concentration solutions, and $FeCl_2^+$, $FeCl_{3(aq)}$ and $FeCl_4^-$ become important as the chloride concentration increases. Note that the borders of the predominance fields of $FeCl_{3(aq)}$ and $FeCl_4^-$ shift towards lower chloride concentration with increasing temperature, indicating that these non-octahedral complexes become more stable at higher temperatures relative to the octahedral complexes.

3.9. Effect of the Setchénow coefficient for $FeCl_{3(aq)}$ on the model

The effect of the Setchénow coefficient for $FeCl_{3(aq)}$, $b_{\gamma,FeCl_{3(aq)}}$, on the speciation model and the quality of the fit was investigated by fitting different values of $b_{\gamma,FeCl_{3(aq)}}$ (Fig. 9). The retained value of 0.1 corresponds to a minimum in residuals (Fig. 9a), while the resulting distribution of species shows the regular succession of Fe(III) chloride complexes also retrieved by the model-free analysis (Figs. 9c and 3). Large values of $b_{\gamma,FeCl_{3(aq)}}$ (e.g., 0.4) result in a significantly higher residual, and also in an unreasonable distribution of species as $FeCl_{3(aq)}$ becomes a very minor species with unrealistically high molar absorptivity coefficients (Fig. 9d). At $b_{\gamma,FeCl_{3(aq)}}$ of 0.025, the residual is also slightly larger, and again the distribution of species differs significantly from that retrieved by the model-free analysis. In particular, the

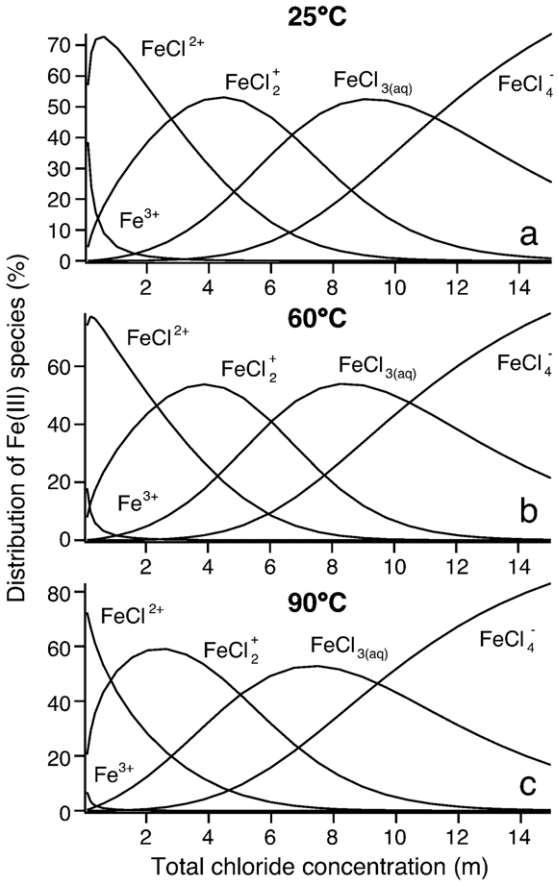

Fig. 8. Distribution of Fe(III) species calculated from the formation constants determined from the analysis of UV–Vis spectrophotometric data at 25, 60 and 90 °C.

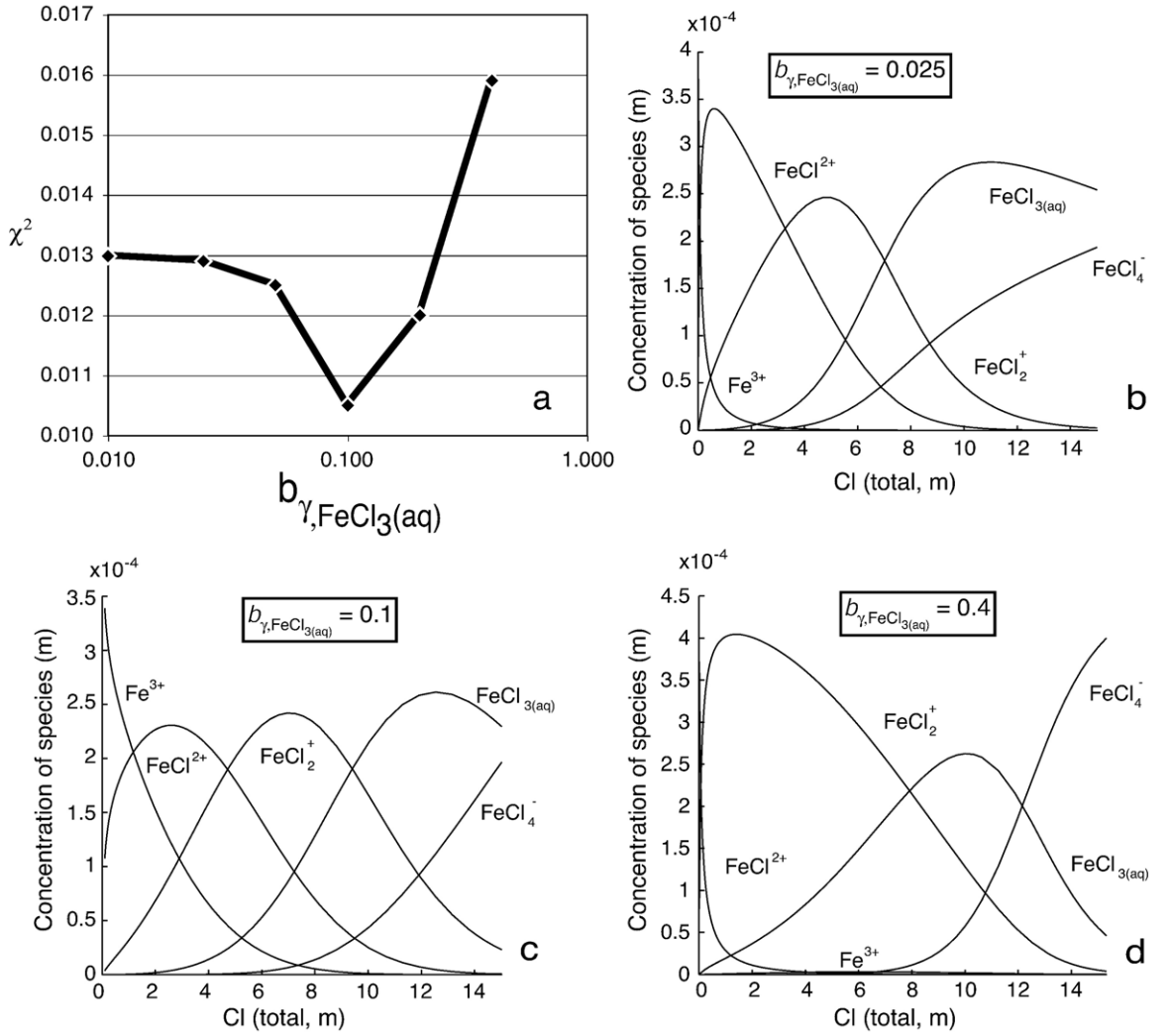

Fig. 9. Effect of the Setchénow coefficient for $FeCl_{3(aq)}$, $b_{\gamma,LiCl_{(aq)}}$, on the model. (a) Residuals as a function of the value for the Setchénow coefficient for $FeCl_{3(aq)}$, $b_{\gamma,LiCl_{(aq)}}$. (b) Distribution of species obtained for $b_{\gamma,LiCl_{(aq)}}=0.025$. (c) Distribution of species obtained for $b_{\gamma,LiCl_{(aq)}}=0.1$. (d) Distribution of species obtained for $b_{\gamma,LiCl_{(aq)}}=0.4$.

distribution of $FeCl_{3(aq)}$ is asymmetric, and tails off only slowly at high chloride concentration to give way to $FeCl_4^-$ (Fig. 9b).

4. Interpretation of XAFS data

XAFS spectroscopy is used to provide confirmation of the speciation model derived from the UV–Vis spectrophotometric experiment and in particular as a test of the validity of the Beer-Lambert law for the studied system, and to further characterise the geometry of the Fe(III) chloride complexes. Structural information can be obtained by comparing XANES spectra of solutions with those obtained on compounds with a known structure. Unique information such as metal-ligand distance and number of ligands can be extracted from the EXAFS oscillations.

4.1. XANES

The XANES spectrum (about 20 eV below to about 30 eV above the absorption edge) arises from the excitation of core electrons to higher electronic states, and contains information about oxidation state and coordination symmetry. The Fe *K* absorption edge can be divided into three distinct regions: the pre-edge $1s\rightarrow 3d$ transition, the shoulder $1s\rightarrow 4s$ transition and the edge crest $1s\rightarrow 4p$ transition (e.g., Waychunas et al., 1983; Wilke et al., 2001; Berry et al., 2003; Fig. 10).

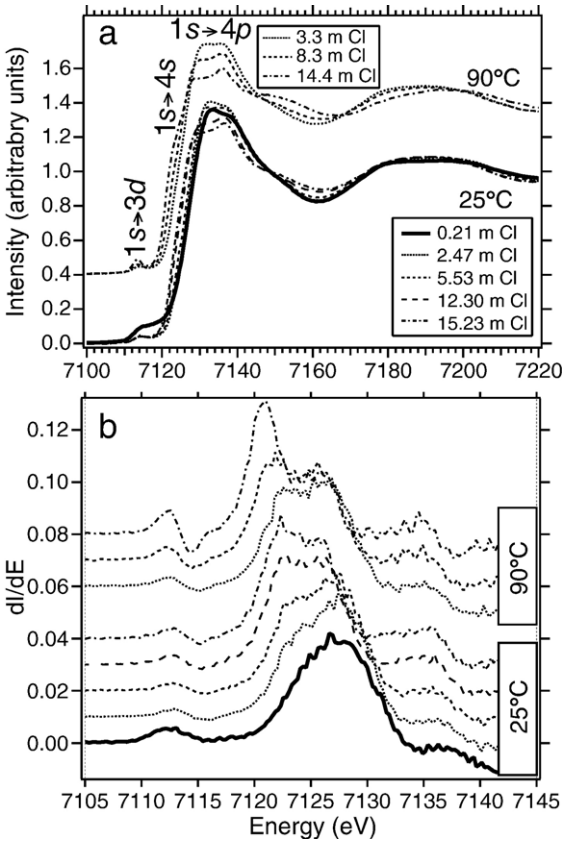

Fig. 10. XANES spectra of Fe(III) chloride solutions. (a) Background-corrected XANES spectra Total chloride concentrations are indicated. (b) First derivative of spectra in (a), showing the edge shift towards low energy with increasing salt concentration and temperature.

Backgrounds were subtracted from the XANES spectra using AUTOBK 2.93a (Newville et al., 1993). AUTOBK fits two different background functions to the pre-and post-edge regions, which results in a discontinuity at the edge. To obtain a smooth background function across the edge, the following procedure was used: (1) The pre-edge AUTOBK background function was shifted such that the $\mu(E)$ at 7060.1 eV was set to zero; (2) similarly, the post-edge AUTOBK background function was shifted such that the $\mu(E)$ at 7167.5 eV was set to zero; (3) between 7060.1 and 7167.5 eV, the background function was assumed to be zero; (4) the step height was then normalized such that the difference in $\mu(E)$ between 7060.1 and 7505 eV was equal to one. This procedure does not formally produce a continuous function, but an acceptable approximation within 0.01 unit (normalized).

The XANES spectra of Fe(III) in solution change with increasing LiCl concentration (Fig. 10), indicating that there is a change in the coordination of Fe. The spectrum for Fe in 0 m LiCl (0.21 m Cl_{tot}) looks slightly different to the other spectra and the pre-edge peak at 7113.5 eV due to the $1s\rightarrow3d$ transition is not as well defined. The XANES spectra are broader than those previously published in the literature (Waychunas et al., 1983; Wilke et al., 2001), as a result of the energy resolution of the beamline optics at BL-20B. The monochromator energy bandpass is 1.87 eV at the Fe *K*-edge; together with the Fe-*K*α core-hole width of 1.25 eV this result in an energy resolution of ~2.2 eV (Berry et al., 2003). The intensity of the $1s\rightarrow3d$ transition increases with increasing LiCl concentration; this trend is more pronounced for the 90 °C spectra. This is consistent with a change in the coordination around Fe going from octahedral to tetrahedral (Waychunas et al., 1983 and references within). Both the 1*s* and 3*d* states are centrosymmetric, thus, quantum mechanical selection rules indicate that there is only a small probability that this transition will occur. However, when Fe is in a tetrahedral, i.e., non-centrosymmtric coordination, the subsequent mixing of 4*p* and 3*d* molecular orbitals allows for an increase in the probability that this transition will occur (e.g. Apted et al., 1985).

The edge and edge crest are shifted systematically to lower energy as the Fe(III) ion is subjected to increasingly concentrated LiCl solutions (Fig. 10b). A similar trend was observed by Apted et al. (1985) for Fe in hypersaline solutions. Such a systematic shift of the edge towards lower energy can be related to a decrease in the effective ionic charge of the metal, as the binding energy of the 1*s* electron decreases due to lower electron–ligand repulsion (Waychunas et al., 1983). However, the substitution of chloride for water molecules results in longer metal-ligand bonds (Table 5), and hence in higher effective ionic charge for the metal (Suchet, 1965). Most likely, the observed decrease in the energy of the edge crest by ~4–5 eV is due to the higher intensity of a satellite band of the $1s\rightarrow4p$ transition, hidden due to the relatively low resolution of our measurements. A similar explanation was offered by Waychunas et al. (1983) to explain a −5 eV shift of the edge crest in XANES spectra of Fe(II) compounds as Fe–O distances vary from 1.95 to 2.25 Å. A shoulder at the energy expected for the $1s\rightarrow4s$ band can be seen on the XANES spectra collected at the highest salt concentrations (Fig. 10a). This may account for the observed shift, as the intensity of this symmetric transition is expected to be much higher in a tetrahedral (asymmetric) state compared to the symmetric octahedral state. The amplitude of the edge-crest decreases with increasing LiCl concentration and the ‘slope of the

Table 4
Coordination number and bond lengths for Fe in LiCl solutions at room temperature and 90°C

Solution name	T (°C)	Model	N1† calc [O_{oct}]	O_{tet}	N2† calc [Cl_{oct}]	N3† calc [Cl_{tet}]	N1* [O_{oct}]	N2* [Cl_{oct}]	N3* [Cl_{tet}]	X1* (Å)	Y2* (Å)	Z*3 (Å)	δ1* (Å^2)	δ2* (Å^2)	δ3* (Å^2)	χ^{2*}
0 m	**25**	**Oct.**	**5.41**		**0.59**		**5.78 (0.26)**	**0.22 (0.26)**		**2.00 (0.01)**	**2.26 (0.06)**		**0.0036 (0.0010)**	**0.0002 (0.0001)**		**6.28**
0 m	25	Tet.	–		–		4.0 (0.26)	0.0 (0.26)		2.00 (0.01)			0.0016 (0.0010)			17.6
2 m	**25**	**Oct.**	**4.43**		**1.48**		**4.64 (0.99)**	**1.36 (0.99)**		**1.99 (0.02)**	**2.24 (0.02)**		**0.0033 (0.0011)**	**0.0019 (0.0037)**		**8.08**
2 m	25	Tet.	–		–		2.75 (0.21)	1.25 (0.21)		1.98 (0.02)	2.24 (0.02)		0.0002 (0.0001)	0.0002 (0.0001)		22.0
15 m	25	Oct.	–		–		3.0	3.0		2.05 (0.02)	2.32 (0.01)		0.0057 (0.0062)	0.0057 (0.0175)		2.02
15 m	25	Tet.–					1.2	2.8		2.05 (0.04)	2.30 (0.02)		0.0002 (0.0001)	0.0002 (0.0001)		2.98
15 m	**25**	**Mixed tet/oct**	**0.7**	**0.00**	**0.7**	**3.0**	**1.5**	**2.0**	**2.6**	**2.02 (0.02)**	**2.33 (0.01)**	**2.23 (0.01)**	**0.006 (0.01)**	**0.002 (0.002)**	**0.006 (0.003)**	**2.28**
2 mli	**90**	**Oct.**	**3.93**		**1.79**		**3.92 (0.96)**	**2.08 (0.96)**		**2.00 (0.01)**	**2.28 (0.01)**		**0.0036 (0.0020)**	**0.0032 (0.0036)**		**5.62**
2 mli	90	Tet.					2.52 (0.32)	1.48 (0.32)		2.00 (0.03)	2.28 (0.02)		0.0002 (0.0001)	0.0002 (0.0001)		9.75
15 mli	90	Oct.					2.12 (0.92)	3.88 (0.92)		2.09 (0.02)	2.21 (0.02)		0.0004 (0.0040)	0.0081 (0.0037)		1.88
15 mli	90	Tet.					1.38 (0.46)	2.62 (0.46)		2.04 (0.03)	2.23 (0.01)		0.0002 (0.0001)	0.0037 (0.0014)		2.41
15 mli	**90**	**Mixed tet/oct**	**0.3**	**0.08**	**0.25**	**3.6**	**0.3**	**0.3**	**3.8**	**2.00 (0.02)**	**2.33 (0.01)**	**2.20 (0.03)**	**0.03 (0.005)**	**0.002 (0.03)**	**0.004 (0.002)**	**0.98**

The preferred models are shown in bold.
† Average number of ligands in the first coordination shell according to the distribution of species shown in Fig. 8, assuming that $FeCl_3$(aq) is octahedral at 25 °C and consists of a 50–50% mixture of octahedral $FeCl_3(OH_2)_{3(aq)}$ and tetrahedral $FeCl_3(OH_2)_{(aq)}$ at 90 °C, and that $FeCl_4^-$ is purely tetrahedral. High correlation among refined parameters in the mixed tet/oct models results in meaningless ($\gg 2$) errors for the number of ligands, and the errors are omitted. *Ligand number (N1, N2 and N3), distances (X1, Y2 and Z3, respectively), Debye-Weller coefficients (δ1, δ2, δ3) and residuals (χ^2) from the EXAFS analysis.

peak' changes from negative (2 and 5 m) to positive (10 and 15 m).

4.2. EXAFS

EXAFS spectra generally refer to the region 30–1000 eV above the absorption edge. The EXAFS spectra represent a final state interference effect arising from the scattering of the outgoing photoelectron from neighbouring atoms. The amplitude and frequency of the sinusoidal modulation of absorbance vs. energy depends on the type and bonding of the neighbouring atom and their distances, thus EXAFS contains information about coordination numbers, distances to neighbouring atoms and bond disorder.

The EXAFS data were refined using XFIT 1.1 (Ellis and Freeman, 1995) with single scattering theory (FEFF version 6, Zabinsky et al., 1995). Self-absorption corrections were applied with SABCOR (Booth and Bridges, 2003) and found to be negligible. The scale factor (S02) of 0.8 was determined from the lowest salinity solution (Fe in 0.11 m LiCl), containing mainly the hexaaquo Fe(III) complex, and this value was used for refinements of all subsequent solutions. The edge energy E_0, number of O and Cl atoms, Debye-Waller factors (δ) for both atom types and the distance from absorber to ligand (X, Y, Z) were refined in both limiting geometries (octahedral and tetrahedral) for Fe in 2 and 15 m LiCl at room temperature and at 90 °C (Table 4; Fig. 11). Constraints were applied so that the refinements converged to physically sensible solutions: $(1.8\pm0.1\ \text{Å}) \le R_{\text{Fe–O}} \le (2.1\pm0.1\ \text{Å})$, $(2.0\pm0.1\ \text{Å}) \le R_{\text{Fe–Cl}} \le (2.4\pm0.1\ \text{Å})$, $(0.0002\pm0.0001\ \text{Å}^2) \le \delta \le (0.03\pm0.005\ \text{Å}^2)$, and the total number of atoms in the first shell was constrained to be either 4 or 6. The refinements were performed on k^3-weighted spectra, in the k-ranges: $2<k<12$ for the ~2 m LiCl solution, and $2<k<9$ for the ~15 m LiCl solution. The spectra for the ~15 m LiCl solution were noisier due to increased absorption of X-rays by the chloride-rich matrix, hence

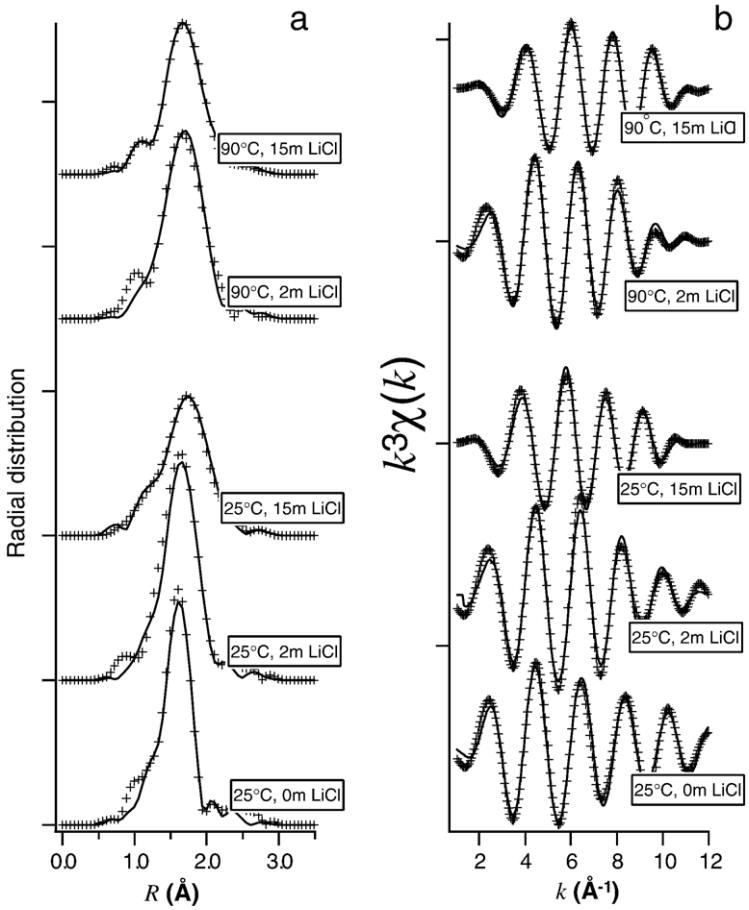

Fig. 11. Filtered and windowed EXAFS data; lines are experimental spectra and crosses are calculated spectra (see Table 4). (a) Fourier transforms of EXAFS spectra for Fe(III) solutions at 25 and 90 °C. (b) EXAFS spectra for Fe(III) solutions at 25 and 90 °C.

Table 5
Average Fe(III)–O and Fe(III)–Cl distances in monomeric coordination compounds (from Melnik et al., 1997)

	Fe(III)–O	Fe(III)–Cl
Octahedral geometry	2.05 Å	2.29 Å
Trigonal dipyramidal	2.11 Å (axial)	2.20 Å (equatorial)
Tetrahedral geometry	1.88 Å	2.18 Å

Trigonal dipyramidal distances are for the compound $FeCl_3(thf)_2$ (Ivakina et al., 1987).

limiting the *k*-range useable in the analysis. Results are tabulated in Table 4.

Fe in the 0.11 m LiCl solution at 25 °C is octahedrally coordinated to six O, with only a small fraction of coordinated Cl as expected from calculations using the log*K*'s in Table 3. The tetrahedral model can be rejected on the basis of high residuals. The Fe–O distance of 2.00(1) Å is shorter than the distance (2.10 Å) obtained from EXAFS spectra of a highly concentrated solution (1 m Fe(III), 7.8 m Cl; Apted et al., 1985), and the distance calculated by Harris et al. (1997) for the $Fe(OH_2)_6^{3+}$ complex (2.06–2.09 depending on the model used). However, this distance is similar to the average Fe–OH_2 distance measured in highly hydrated Fe(III) sulfates (1.99(4) Å in quenstedtite, Thomas et al., 1974; 1.98(2) Å in paracoquimbite, Robinson and Fang, 1971), to previous experimental studies listed by Ohtaki and Radnai (1993; 2.01–2.05 Å), and to a recent ab initio calculation results of Fe–O distance for $Fe(H_2O)_6^{3+}$ (2.03–2.04, Kubicki, 2001). The Fe–Cl distance of 2.26(6) Å is also in the range expected for an octahedral compound (average Fe–Cl distance 2.29 Å; Table 5).

In the 2 m LiCl solution at 25 and 90 °C, Fe is still clearly octahedrally coordinated, and the number of Cl ligands in the first coordination sphere increases as expected from the UV–Vis study (Fig. 8). The Fe–O distances are identical within error at both temperatures and in the 0.11 m LiCl solution. The precision of the Fe–Cl distance is better than in the 0.11 m LiCl solution due to higher Cl content in the first coordination sphere; however, the precision is still too poor to observe a change with temperature: 2.24(2) Å at 25 °C and 2.28(2) Å at 90 °C, i.e. overlapping at the 2-σ level.

At 15 m LiCl both the octahedral and tetrahedral models result in acceptable fits, though the lowest residuals are obtained for the octahedral models (e.g., $\chi^2_{tetr}=2.98$ and $\chi^2_{oct}=2.02$ at 25 °C). The retrieved Fe–O and Fe–Cl distances are suggestive of an octahedral coordination (Tables 6 and 7); only the Fe–Cl distance at 90 °C could be related to a tetrahedral compound. Maps of the X^2 function minimised by Xfit as a function of the Cl/O ratio and Fe–O and Fe–Cl distances were drawn to explore the possibility of an alternative local minimum corresponding to a tetrahedral complex; however, no significantly better tetrahedral solution could be found. This result appears to contradict the XANES and UV–Vis data, which clearly indicate a change in the geometry of the complex with increasing salinity. Moreover, the $FeCl_4^-$ group is very common in coordination compounds (Melnik et al., 1997), and such a complex in expected in highly saline brines.

To resolve this problem, we tested the hypothesis that some of the $FeCl_{3(aq)}$ and possibly some of the $FeCl_4^-$ may exist as an octahedral complex, i.e. these complexes are a mixture of octahedral and tetrahedral forms. The new model contains three shells: O in octahedral coordination, Cl in tetrahedral coordination, and Cl in octahedral coordination. O in tetrahedral coordination has been neglected because only small quantities (less than 0.1 in the proposed models; Table 4). The Fe–O and Fe–Cl distances were constrained to be in an acceptable range for the given geometry (Table 5).

At 25 °C, the model converges for relatively high proportion of octahedral O and Cl (Table 4). Such high values require that both $FeCl_{3(aq)}$ and $FeCl_4^-$ consist of a mixture of octahedral and tetrahedral forms. At 90 °C, however, the model gives excellent agreement with the speciation derived from the UV–Vis experiment if it is assumed that $FeCl_{3(aq)}$ consists of a 1:1 mixture of the octahedral and tetrahedral forms, while $FeCl_4^-$ is probably tetrahedral (Table 4). Hence, the EXAFS data

Table 6
Comparison of stepwise formation constants for Fe(III) chloride complexes

Author	Method	Medium	*T* (°C)	$\log K_{FeCl_2^+}$	$\log K_{FeCl_{3(aq)}}$	$\log K_{FeCl_4^-}$
Rabinowitch and Stockmayer (1942)	Spectrophotometry	$HClO_4$	25	0.11±0.25	−1.0±0.2	
Gamlen and Jordan, 1953	Spectrophotometry	HCl	20		−0.14	−1.98
Marcus, 1960	Anion exchange	HCl	25		−1.40±0.04	−1.92±0.08
Tagirov et al., 2000	Potentiometry	$HClO_4$	25	0.9±0.2		
This study	Spectrophotometry	HCl	25	0.32±0.25	−1.11±0.4	−2.03±0.3
			60	0.49±0.25	−0.97±0.3	−1.93±0.3
			90	0.95±0.45	−0.63±0.55	−1.79±0.45

Table 7
Parameters of the density model regressed from the experimental data of this study for $FeCl_2^+$, $FeCl_{3(aq)}$ and $FeCl_4^-$, and from Tagirov et al.'s (2000) experimental data for $FeCl^{2+}$

Reaction	p_1	p_2	p_3
$Fe^{3+}+Cl^-=FeCl^{2+}$	−8.6864	1584.1	12961.5
$Fe^{3+}+2Cl^-=FeCl_2^+$	3.3456	−2121.0	54358.9
$Fe^{3+}+3Cl^-=FeCl_{3(aq)}$	14.930	−4724.0	84870.1
$Fe^{3+}+4Cl^-=FeCl_4^-$	21.458	−5247.7	94873.0

provide additional support for the increase in stability of the tetrahedral ferric iron chloride complexes with increasing temperature. Note that EXAFS is not able to distinguish between a tetrahedral or trigonal dipyramidal geometry for $FeCl_{3(aq)}$. Trigonal dipyramidal $[FeCl_3(H_2O)_2]_{(aq)}$ is found in $FeCl_3$(tetrahydrofuran)$_2$, and features Fe–Cl distances similar to the tetrahedral distances. Moveover, $FeCl_{3(aq)}$ never accounts for more than 60% of the iron in solution (Fig. 8).

5. Discussion

5.1. Speciation of Fe(III) in acidic chloride brines

The speciation model proposed from the literature and UV–Vis experiments involves five species: Fe^{3+}, $FeCl^{2+}$, $FeCl_2^+$, $FeCl_{3(aq)}$ and $FeCl_4^-$. The octahedral geometry of the first three complexes is well established and a change in geometry between $FeCl_2^+$ and $FeCl_{3(aq)}$ is indicated independently by the UV–Vis and XANES data. The EXAFS data suggest that $FeCl_{3(aq)}$ is likely to consist of a mixture of octahedral and tetrahedral or trigonal dipyramidal forms at 25 °C, whereas the tetrahedral or trigonal dipyramidal form predominates at 90 °C. The EXAFS data do not allow to distinguish between tetrahedral and trigonal geometries for $FeCl_{3(aq)}$, but are consistent with tetrahedral geometry for $FeCl_4^-$. These two last species contain less water ligands than the octahedral species and they become more stable with increasing temperature and with increasing chloride concentration relative to the octahedral species.

5.2. Comparison of the formation constants with previous studies

There are no experimentally derived formation constants for the three Fe(III) chloride complexes ($FeCl_2^+$, $FeCl_{3(aq)}$ and $FeCl_4^-$) at elevated temperature. In addition, it is hard to directly compare our derived log$K$ values for Fe(III) chloride complexes with most previous studies as they were often reported at a particular ionic strength. Therefore the comparison here is limited to a few room temperature studies that reported stepwise formation log$K$ values at zero ionic strength (Table 6). The formation constants generated from this study are also shown as stepwise form (e.g., $FeCl_2^+ + Cl = FeCl_{3(aq)}$) in Table 6. For $FeCl_2^+$, our result is about half a log unit lower than Tagirov et al. (2000)'s value, but their values are regressed from previous studies at higher ionic strengths that are in poor agreement (see Fig. 10 in Tagirov et al., 2000). Our value for $FeCl_{3(aq)}$ at 25 °C (−1.11) agree well with the value of Rabinowitch and Stockmayer (1942) and Marcus (1960). These three values differ by about one log unit with Gamlen and Jordan's (1953) values. Our results for $FeCl_4^-$ at 25 °C are −2.03, in excellent agreement with the values of Gamlen and Jordan (1953) and Marcus (1960) (Table 6).

5.3. Extrapolation to higher temperatures

In order to extrapolate formation constants for Fe(III) chloride complexes to temperatures higher than experimental conditions, the density model (Anderson et al., 1991) equation was fitted to the experimentally derived log$K$ values of Fe(III) complexes:

$$\log K = -\frac{1}{2.303}\left[p_1 + \frac{p_2}{T} + \frac{p_3 \ln \rho_w}{T}\right] \quad (14)$$

where ρ_w is density (g/cm^3) of pure water at temperature (T) in Kelvin, taken from Lemmon et al. (2000); p_1, p_2 and p_3 are constants characteristic of each chemical reaction, and were fitted from the experimental log$K$ values of $FeCl_2^+$, $FeCl_{3(aq)}$ and $FeCl_4^-$. We also used this equation to extrapolate Tagirov et al.'s (2000) experimental data. The result is shown in Fig. 5 together with Tagirov et al.'s (2000) extrapolation using a polynomial function. It can be seen that there is an excellent agreement between the two extrapolation approaches.

The fitted parameters p_1, p_2 and p_3 are listed in Table 7, and the extrapolated formation constants for $FeCl^{2+}$, $FeCl_2^+$, $FeCl_{3(aq)}$ and $FeCl_4^-$ are listed in Table 8. With these data, one can model Fe(III) speciation in hydrothermal chloride solutions at temperatures up to 300 °C.

5.4. Geological implications

Activity–activity diagrams were calculated using the properties of Fe(III) chloride complexes derived in this paper and properties of other species listed in the Lawrence Livermore National Laboratory database version 8, revision 6 as implemented in the software

Table 8
Extrapolated logarithms of formation constants for Fe(III) chloride complexes

Temperature (°C)	$Fe^{3+}+Cl^{-}=FeCl^{2+}$	$Fe^{3+}+2Cl^{-}=FeCl_2^{+}$	$Fe^{3+}+3Cl^{-}=FeCl_{3(aq)}$	$Fe^{3+}+4Cl^{-}=FeCl_4^{-}$
25	1.52	1.87	0.77	−1.26
50	1.85	2.28	1.24	−0.73
100	2.57	3.71	3.22	1.49
150	3.30	5.56	5.91	4.50
200	4.05	7.75	9.18	8.16
250	4.87	10.44	13.25	12.72
300	5.91	14.13	18.92	19.06

package Geochemist's Workbench version 3.2.2 (Bethke, 1996). The diagrams in Fig. 12 illustrate the increased stability of the high order, non-octahedral $FeCl_{3(aq)}$ and $FeCl_4^-$ complexes at elevated temperature, even at low chloride concentration (0.1 m). This is consistent with the Raman study by Murata et al. (1989) that suggests that tetrahedral $FeCl_4^-$ predominates at 300 °C in solutions with chloride concentration greater than 3 m. A major geochemical consequence of this is that at elevated *T*, the solubility of hematite does not decrease as dramatically under oxidising (Fe(III) stable) conditions than under reducing (Fe(II) stable) conditions. Also, the stability of the high order Fe(III) chloride complexes $FeCl_{3(aq)}$ and $FeCl_4^-$ probably plays a significant role in enhancing the kinetics of the precipitation of hematite and magnetite from hydrothermal solutions. The stability of these species in brines at room temperature will also affect the bioavailabity and mobility of Fe, as sorption of the neutral or negatively charged species with tetrahedral and/or trigonal dipyramidal geometry will differ fundamentally from that of the positively charged octahedral Fe(III) chloride complexes.

Hematite solubility in acid solutions was calculated as a function of temperature up to 300 °C and at water-saturated pressures, similar to Tagirov et al.'s (2000) calculation. The calculations were conducted using the HCh software (Shvarov and Bastrakov, 1999), using the thermodynamic properties for hematite from Berman (1988) and for $FeOH^{2+}$ from Shock et al. (1997). The

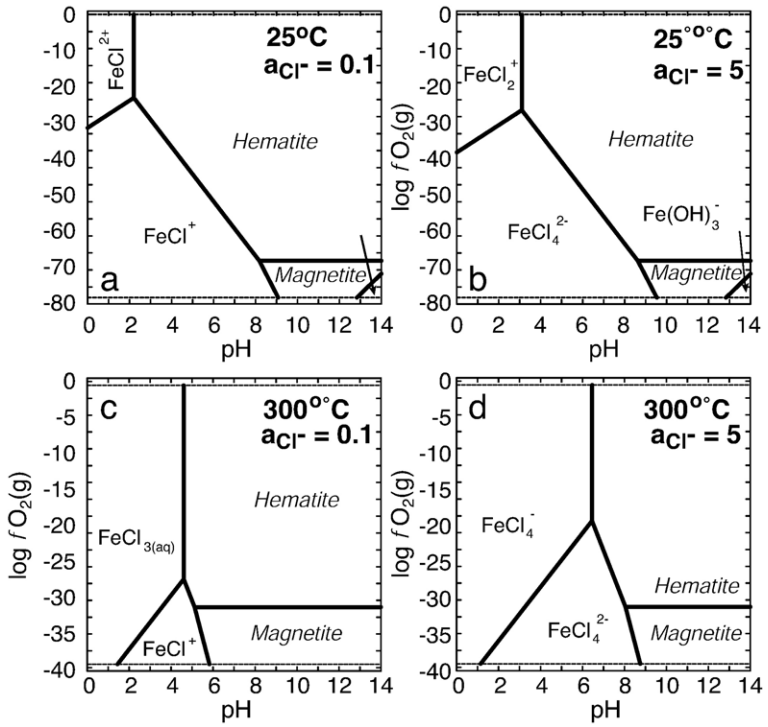

Fig. 12. logf_{O_2}(g) vs. pH activity diagrams for iron speciation in brines at 25 °C (a and b), and at 300 °C (c and d).

results from two different speciation models are reported on Fig. 13. The first model contains only two Fe(III) chloride complexes ($FeCl^{2+}$ and $FeCl_2^+$; thermodynamic properties from Tagirov et al., 2000). The second model includes all four Fe(III) chloride complexes discussed in this paper ($FeCl^{2+}$, $FeCl_2^+$, $FeCl_{3(aq)}$ and $FeCl_4^-$; thermodynamic properties from Table 8). It can be seen from Fig. 13a that hematite solubility decreases with increasing temperature when only $FeCl^{2+}$ and $FeCl_2^+$ are included in the model, but when the high order Fe(III) chloride complexes ($FeCl_{3(aq)}$ and $FeCl_4^-$) are also included, the hematite solubility first decreases between 25 °C and 125 °C, then increases from 125 °C. The hematite solubilities predicted by both models differ by more than one order of magnitude at temperatures higher than 200 °C. The speciation of Fe(III) species (Fig. 13b) clearly shows that the high solubility at high temperature is due to $FeCl_{3(aq)}$ that predominates in the solution at the higher temperatures. Therefore, it is suggested that high order complexes probably play an important role in controlling the solubility of Fe minerals in oxidised hydrothermal solutions, even at low chloride concentrations. It should be noted that, as Tagirov et al. (2000) stated, available experimental hematite solubility data

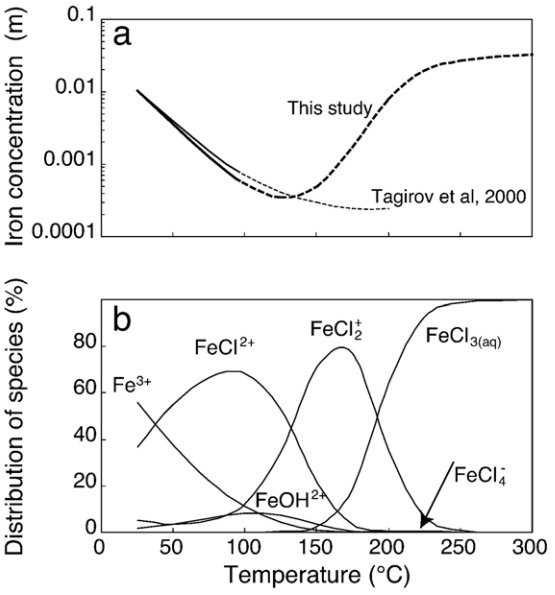

Fig. 13. Solubility of hematite (a) and speciation of Fe(III) complexes (b) in 0.1 m HCl solutions as a function of temperature between 25–300 °C. The thick line in (a) was calculated including $FeCl^{2+}$, $FeCl_2^+$, $FeCl_{3(aq)}$ and $FeCl_4^-$ complexes. The thin line was calculated only including $FeCl^{2+}$ and $FeCl_2^+$ complexes. The solid part of these lines is within the temperature range (up to 90 °C) of experimental data, and dashed part is calculated using extrapolated log$K$ values listed in Table 8.

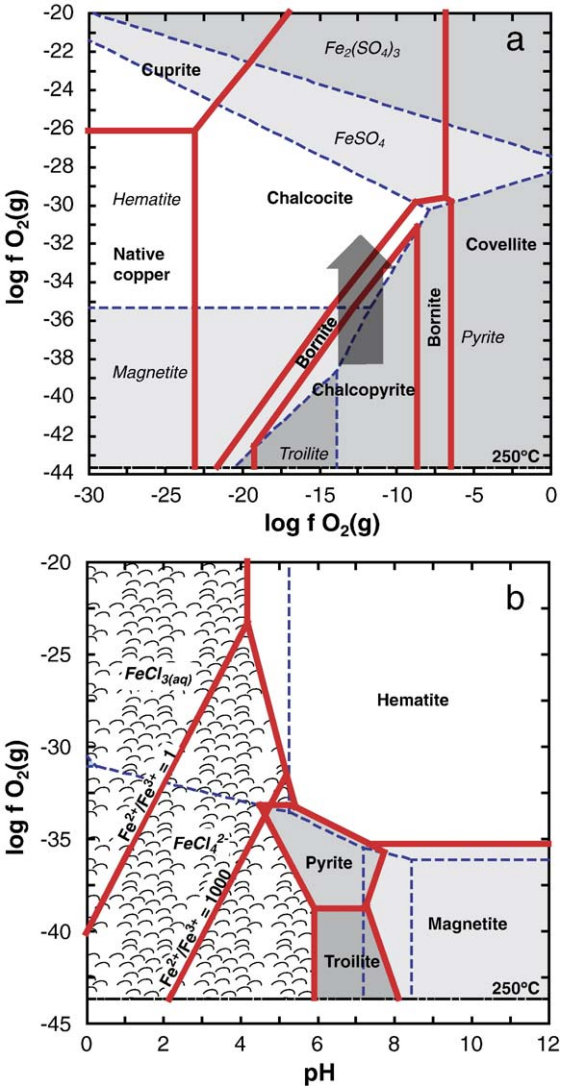

Fig. 14. Fe speciation in Olympic Dam type fluids, under conditions similar to those proposed by Haynes et al. (1995). (a) Phase relationships in the Fe–Cu–S–O–H system at 250 °C at P_{sat}=39.83 bars. The diagram for Fe is shaded. The arrow shows the paragenetic trend observed at Olympic Dam. $a_{Fe}=10^{-5.4}$, $f_{H_2S}(g)=10^{-2.8}$, $a_{Cl^-}=10^{-0.2}$ (corresponding to 3.5 m Cl_{tot}). (b) log$f$ O_2(g) versus pH solubility diagram for Fe minerals. The sub-diagram for sulphur is plotted using dashed lines.

up to 200 °C are not consistent with calculated ones, probably due to the non-equilibrium in the experiments and formation of amorphous iron hydroxides. Therefore the reliability of the extrapolation awaits verification with high temperature experimental data, preferably using spectroscopy or potentiometric methods that are not affected by problems encountered in solubility experiments.

The giant Olympic Dam Cu-U-Au-REE-deposit (South Australia; Haynes et al., 1995) represents the

best known-example of hematite-dominated iron oxide copper gold deposit. The evolution of the mineralogical associations at Olympic Dam, from chalcopyrite + magnetite + pyrite to bornite + hematite to chalcocite + hematite, can be related to an increase in $fO_2(g)$ driven for example by fluid mixing (Fig. 14a). Haynes et al. (1995) used numerical geochemical modelling to test this hypothesis: assuming mixing of a reduced magmatic or deeply circulated meteoritic water with a more oxidised, cooler meteoritic water. Calculations of Fe speciation for the deep brine (Fig. 14b) suggest that even in this relatively reduced fluid, a small but significant amount of Fe (~1‰) exists as Fe^{3+}. Note that $FeCl_{3(aq)}$ is predicted to be the predominant Fe^{3+} complex in this simulation, because Geochemist's Workbench uses the Helgeson "*b*-dot" equation to calculate activity coefficients, and this is not accurate for salt concentrations above ~1 m, and underestimates the values of the Cl^- activity.

These calculations illustrate the fact that due to their increasing stability at increasing temperature, the high order Fe(III)-chloride complexes may play a more important role than expected in hydrothermal systems. Even small amounts of Fe(III) in solution may have significant implication for the mineralogy of the ore deposit, by favouring the kinetics of precipitation of Fe(III)-bearing phases (e.g., hematite, magnetite) and possibly acting as an oxidant for other metals.

6. Conclusions and perspectives

The UV–Vis and XAFS spectra of Fe(III) chloride solutions have been measured between temperatures of 25 °C and 90 °C. The speciation model and the structure of Fe(III) chloride complexes were examined by synchrotron XAFS experiments, and the equilibrium constants for Fe(III) chloride complexes were regressed from the UV spectrophotometric data.

The UV spectra of ferric solutions change systematically with increasing chloride concentration and increasing temperature. Quantitative interpretation of the spectra shows that $FeCl^{2+}$, $FeCl_2^+$, $FeCl_{3(aq)}$ and $FeCl_4^-$ were present under the experimental conditions. As chloride concentrations increase, complexes containing a higher number of ligated chlorides become more important, with $FeCl_4^-$ predominating in solutions with chloride concentrations greater than 10 m at 25 °C. Increasing temperature increases the predominant fields of tetrahedral or trigonal dipyramidal $FeCl_{3(aq)}$ and tetrahedral $FeCl_4^-$. Refinement of the EXAFS spectra suggests that $FeCl_{3(aq)}$ evolve from a mixture of octahedral–tetrahedral or trigonal dipyramidal form at 25 °C to predominantly tetrahedral or trigonal dipyramidal at 90 °C.

The formation constants for ferric chloride complexes determined from the UV data generally show a good agreement with previous room temperature studies. Based on the variable temperature experimental data generated from this and previous studies, extrapolation of log K for ferric chloride complexes to 300 °C shows that high order complexes become stronger with increasing temperature. Using the extrapolated log*K* data, the calculated hematite solubility at temperatures greater than 150 °C is much higher than previously estimated, and the high order complexes $FeCl_{3(aq)}$ and $FeCl_4^-$ are predicted to be predominant at these temperatures even in relatively low chloride concentration solutions. Although the extrapolation still needs to be confirmed by high temperature experiments, it is clear that the high order complexes $FeCl_{3(aq)}$ and $FeCl_4^-$ should clearly be included in the modelling of iron transport in oxidised hydrothermal brines.

This study demonstrates that in spite of the fundamental difficulties of studying hypersaline solutions (activity–compositions relationships; experimental limitations), it is possible to build speciation models that are consistent over the whole range of salt concentrations and with all available experimental data, while being easily implemented in popular geochemical modelling software. The fundamental information that we are gaining on the speciation of trace elements in brines will help to develop more reliable theoretical and experimental frameworks for the study of these systems in the context of ore formation and environmental geochemistry.

Acknowledgement

We would like to thank Mike Shelley for building the titanium cell, James Hester for helping to set up the experiments at the Photon Factory, Corwin Booth for assistance with SABCOR and Jay Black for preparing the Li-triflate and providing unpublished density data. This study was supported by the Australian Research Council (DP0208323) and by the Australian Synchrotron Research Program (Fellowship to B.E.). This manuscript benefited from comments from Glen Waychunas and four anonymous reviewers. **[DR]**

References

Anderson, G.M., Castet, S., Schott, J., Mesmer, R.E., 1991. The density model for estimation of thermodynamic parameters of reactions at high temperatures and pressures. Geochimica et Cosmochimica Acta 55, 1769–1779.

Apted, M.J., Waychunas, G.A., Brown, G.E., 1985. Structure and specification of iron complexes in aqueous solutions determined by X-ray absorption spectroscopy. Geochimica et Cosmochimica Acta 49, 2081–2089.

Baes, C.F.J., Mesmer, R.E., 1976. The Hydrolysis of Cations. Wiley-Interscience.

Berman, R.G., 1988. Internally-consistent thermodynamic data for minerals in the system Na_2O–K_2O–CaO–MgO–FeO–Fe_2O_3–Al_2O_3–SiO_2–TiO_2–H_2O–CO_2. Journal of Petrology 29, 445–522.

Berry, A.J., O'Neill, H.S.C., Jayasuriya, K.D., Campbell, S.J., Foran, G.J., 2003. XANES calibrations for the oxidation state of iron in a silicate glass. American Mineralogist 88, 967–977.

Bethke, C.M., 1996. Geochemical Reaction Modeling; Concepts and Applications, p. 397.

Bjerrum, J., Halonin, A.S., Skibsted, L.H., 1975. Studies of cobalt(II) halide complex formation: I. A spectrophotometric study of the chloro cobalt(II) complexes in strong aqueous chloride solutions. Acta Chemica Scandinavia A29, 326–332.

Booth, C.H., Bridges, F., 2003. SABCOR. Improved self-absorption correction for fluorescence measurements of extended x-ray absorption fine-structure. The 12th International Conference on X-Ray Absorption Fine Structure (XAFS XII). Vol. http://lise.lbl.gov/RSXAP/.

Bray, W.C., Hershey, A.V., 1934. The hydrolysis of ferric ion. The standard Potential of the ferric-ferrous electrode at 25. The equilibrium $Fe^{3+}+Cl^{-}=FeCl^{2+}$. Journal of the American Chemical Society 56, 1889–1893.

Brubaker, G.R., Peterson, R.A., 1989. Stability of the monochloroiron (III) cation in aqueous solutions between 298 and 398 K. Inorganica Chimica Acta 155, 139–144.

Brugger, J., McPhail, D.C., Black, J., Spiccia, L., 2001. Complexation of metal ions in brines: application of electronic spectroscopy in the study of the Cu(II)–LiCl–H_2O system between 25 and 90 °C. Geochimica et Cosmochimica Acta 65, 2691–2708.

Byrne, R.H., Kester, D.R., 1976. A potentiometric study of ferric ion complexes in synthetic media and seawater. Marine Chemistry 4, 275–287.

Byrne, R.H., Kester, D.R., 1981. Ultraviolet spectroscopic study of ferric equilibriums at high chloride concentrations. Journal of Solution Chemistry 10, 51–67.

Byrne, R.H., Luo, Y.R., Young, R.W., 2000. Iron hydrolysis and solubility revisited: observations and comments on iron hydrolysis characterizations. Marine Chemistry 70, 23–35.

Clifford, A.A., Crawford, B.J., 1966. Vibrational intensities: XIV. The relation of optical constants to molecular parameters. Journal of Physical Chemistry 70, 1536–1543.

De Juan, A., Vander Heyden, Y., Tauler, R., Massart, D.L., 1997. Assessment of new constraints applied to the alternating least squares method. Analytica Chimica Acta 346, 307–318.

Draper, N.R., Smith, H., 1998. Applied Regression Analysis. Wiley-Intersciences.

Ellis, P.J., Freeman, H.C., 1995. Xfit—an interactive EXAFS analysis program. Journal of Synchrotron Radiation 2, 190–195.

Friedman, H.L., 1952. The visible and ultraviolet absorption spectrum of the tetrachloroferrate(III) ion in various media. Journal of the American Chemical Society 74, 5–10.

Gamlen, G.A., Jordan, D.O., 1953. A spectrophotometric study of the iron(III) chloro-complexes. Journal of Chemical Society 1953, 1435–1443.

Harris, D., Loew, G.H., Komornicki, A., 1997. Structure and relative spin-state energetics of $Fe(H_2O)_6^{3+}$: a comparison of UHF, Moller-Plesset, nonlocal DFT, and semiempirical INDO/S calculations. Journal of Physical Chemistry A 101, 3959–3965.

Haynes, D.W., Cross, K.C., Bills, R.T., Reed, M.H., 1995. Olympic dam ore genesis—a fluid-mixing model. Economic Geology 90, 281–307.

Heinrich, C.A., Seward, T.M., 1990. A spectrophotometric study of aqueous iron(II) chloride complexing from 25 to 200 °C. Geochimica et Cosmochimica Acta 54, 2207–2221.

Heistand, R.N., Clearfield, A., 1963. The effect of specific swamping electrolytes upon the formation constant of the monochloroiron (III) complex. Journal of the American Chemical Society 85, 2566–2570.

Helgeson, H., Kirkham, D.H., 1974. Theoretical prediction of the thermodynamic behavior of aqueous electrolytes at high pressures and temperatures: II. Debye-Hückel parameters for activity coefficients and relative partial molal properties. American Journal of Science 274, 1199–1261.

Holmes, H.F., Mesmer, R.E., 1983. Thermodynamic properties of aqueous solutions of the alkali metal chlorides to 250 °C. Journal of Physical Chemistry 87, 1242–1255.

Inada, Y., Funahashi, S., 1999. Equilibrium and structural study of chloro complexes of iron(III) ion in acidic aqueous solution by means of X-ray absorption spectroscopy. Zeitschrift Fur Naturforschung. B, A Journal of Chemical Sciences 54, 1517–1523.

Ivakina, L.V., Streltsova, N.R., Belskii, V.K., Storozhenko, P.A., Bulychev, B.M., Tarasov, A., 1987. Structure and properties of ferric-chloride solvates with tetrahydrofuran and 15-crown-5. Zhurnal Obshchei Khimii 57, 1600–1605.

Johnson, J.W., Oelkers, E.H., Helgeson, H.C., 1992. SUPCRT92; a software package for calculating the standard molal thermodynamic properties of minerals, gases, aqueous species, and reactions from 1 to 5000 bar and 0 to 1000 °C. Computers & Geosciences 18, 899–947.

Kielland, J., 1937. Individual activity coefficients of ions in aqueous solutions. Journal of the American Chemical Society 59, 1675–1678.

Kubicki, J.D., 2001. Self-consistent reaction field calculations of aqueous Al^{3+}, Fe^{3+}, and Si^{4+}: calculated aqueous-phase deprotonation energies correlated with experimental $In(K_a)$ and pK_a. Journal of Physical Chemistry A 105, 8756–8762.

Lemmon, E.W., McLinden, M.O., Friend, D.G., 2000. Thermophysical properties of fluid systems. In: Mallard, W.G., Linstrom, P.J. (Eds.), NIST Chemistry WebBook, NIST Standard Reference Database, vol. 69. National Institute of Standards and Technology. http://webbook.nist.gov.

Lide, D.R., 2003. CRC Handbook of Chemistry and Physics. CRC Press. 2616 pp.

Liu, W., McPhail, D.C., Brugger, J., 2001. An experimental study of copper(I)-chloride and copper(I)-acetate complexing in hydrothermal solutions between 50 °C and 250 °C and vapor-saturated pressure. Geochimica et Cosmochimica Acta 65, 2937–2948.

Liu, W., Brugger, J., McPhail, D.C., Spiccia, L., 2002. A spectrophotometric study of aqueous copper(I)–chloride complexes in LiCl solutions between 100 °C and 250 °C. Geochimica et Cosmochimica Acta 66, 3615–3633.

Malinowski, E.R., Howery, D.G., 1980. Factor Analysis in Chemistry. John Wiley and Sons.

Marcus, Y., 1960. The anion exchange of metal complexes: IV. The iron(III)–chloride system. Journal of Inorganic & Nuclear Chemistry 12, 287–296.

Melnik, M., Ondrejkovicova, I., Vancova, V., Holloway, C.E., 1997. Structural aspects of iron coordination compounds: 1. Monomeric derivatives. Reviews in Inorganic Chemistry 17, 55–286.

Meloun, M., Capek, J., Miksik, P., Brereton, R.G., 2000. Critical comparison of methods predicting the number of components in spectroscopic data. Analytica Chimica Acta 423, 51–68.

Millero, F.J., Yao, W.S., Aicher, J., 1995. The speciation of Fe(II) and Fe(III) in natural waters. Marine Chemistry 50, 21–39.

Moller, M., 1937. The complex formation of ferric ions with chloride ions. Journal of Physical Chemistry 41, 1123–1127.

Murata, K., Irish, D.E., Toogood, G.E., 1989. Vibrational spectral studies of solutions at elevated temperatures and pressures: 11. A Raman spectral study of aqueous iron(III) chloride solutions between 25 and 300°C. Canadian Journal of Chemistry 67, 517–524.

Newville, M., Livins, P., Yacoby, Y., Rehr, J.J., Stern, E.A., 1993. Near-edge X-ray-absorption fine-structure of Pb—a comparison of theory and experiment. Physical Review B 47, 14126–14131.

Ohtaki, H., Radnai, T., 1993. Structure and dynamics of hydrated ions. Chemical Reviews 93, 1157–1204.

Peck, A.J., Hatton, T., 2003. Salinity and the discharge of salts from catchments in Australia. Journal of Hydrology 272, 191–202.

Rabinowitch, E., Stockmayer, W.H., 1942. Association of ferric ions with chloride, bromide and hydroxyl ions (A spectroscopic study). Journal of the American Chemical Society 64, 335–347.

Rao, D.V.K., Rao, P.T., 1971. Complex band spectrum of iron monochloride in the ultraviolet region. Indian J. Pure Appl. Phys., vol. 9, pp. 102–105.

Robinson, P.D., Fang, J.H., 1971. Crystal structures and mineral chemistry of hydrated ferric sulphates: II. The crystal structure of paracoquimbite. American Mineralogist 56, 1567–1572.

Rowley, J.K., Sutin, N., 1970. The formation and dissociation of monochloroiron(III) at high ionic strengths: equilibrium and kinetic measurements. Journal of Physical Chemistry 74, 2034–2054.

Setchénow, M., 1889. Über die Konstitution der Salzlösungen auf grand ihres Verhaltens zu Kohlensaure. Zeitschrift für Physikalische Chemie 4, 117–126.

Seward, T.M., Henderson, C.M.B., Charnock, J.M., Dobson, B.R., 1996. An X-ray absorption (Exafs) spectroscopic study of aquated Ag^{+} in Hydrothermal Solutions to 350 ^{3}C. Geochimica et Cosmochimica Acta 60, 2273–2282.

Shock, E.L., Sassani, D.C., Willis, M., Sverjensky, D.A., 1997. Inorganic species in geologic fluids; correlations among standard molal thermodynamic properties of aqueous ions and hydroxide complexes. Geochimica et Cosmochimica Acta 61, 907–950.

Shvarov, Y.V., Bastrakov, E.N., 1999. HCh, a software package for geochemical equlibrium modeling: user's guide. Record 1999/25. Australian Geological Survey Organisation.

Solbrig, R.M., Duff, L.L., Shriver, D.F., Klotz, I.M., 1982. Raman and infrared-spectroscopy of the oxo-bridged iron(III) complex, $Cl_3Fe–O–FeCl_3^{-2}$ as a spectroscopic model for the oxo bridge in hemerythrin and ribonucleotide reductase. Journal of Inorganic Biochemistry 17, 69–74.

Strahm, U., Patel, R.C., Matijevic, E., 1979. Thermodynamics and kinetics of aqueous iron(III) chloride complexes formation. Journal of Physical Chemistry 83, 1689–1695.

Suchet, J.P., 1965. Physical Chemistry of Semiconductors. Van Nostrand.

Susak, N.J., Crerar, D.A., 1985. Spectra and coordination changes of transition metals in hydrothermal solutions; implications for ore genesis. Geochimica et Cosmochimica Acta 49, 555–564.

Tagirov, B.R., Diakonov, I.I., Devina, O.A., Zotov, A.V., 2000. Standard ferric-ferrous potential and stability of $FeCl^{2+}$ to 90 °C; thermodynamic properties of $Fe^{3+}_{(aq)}$ and ferric-chloride species. Chemical Geology 162, 193–219.

Thomas, J.N., Robinson, P.D., Fang, J.H., 1974. Crystal structures and mineral chemistry of hydrated ferric sulfates: IV. The crystal structure of quenstedtite. American Mineralogist 59, 582–586.

Waychunas, G.A., Apted, M.J., Brown Jnr., G.E., 1983. X-ray K-edge absorption spectra of Fe minerals and model compounds: near-edge structure. Physics and Chemistry of Minerals 10, 1–9.

Waychunas, G.A., Brown, G.E.J., Apted, M.J., 1986. X-ray K-edge absorption spectra of Fe minerals and model compounds: II. EXAFS. Physics and Chemistry of Minerals 13, 31–47.

Wilke, M., Farges, F., Petit, P.E., Brown, G.E., Martin, F., 2001. Oxidation state and coordination of Fe in minerals: an FeK-XANES spectroscopic study. American Mineralogist 86, 714–730.

Wolery, T.J., 1992. EQ3NR, A Computer Program for Geochemical Aqueous Speciation-Solubility Calculations: Theoretical Manual, User's Guide, and Related Documentation (Version 7.0). Lawrence Livermore National Laboratory.

Woods, S.M.J.M., O.P., Gallagher, P.K., King, E.L., 1962. Thermodynamics of association of iron(III) ion and chloride ion in aqueous solution. Inorganic Chemistry 1, 55–65.

Zabinsky, S.I., Rehr, J.J., Ankudinov, A., Albers, R.C., Eller, M.J., 1995. Multiple-scattering calculations of X-ray-absorption spectra. Physical Review B 52, 2995–3009.

Zhao, R.H., Pan, P.J., 2001. A spectrophotometric study of Fe(II)-chloride complexes in aqueous solutions from 10 to 100 °C. Canadian Journal of Chemistry 79, 131–144.

Zotov, A.V., Kotova, Z.Y., 1979. Spectrophotometric determination of the 1st constant of hydrolysis of Fe^{3+} ion at 25–80 °C. Geokhimiya 1979, 285–290.

Zotov, A.V., Kotova, Z.Y., 1980. Spectrophotometric determination of the first constant of hydrolysis of Fe^{3+} ion at 80–200 °C. Geokhimiya 1980, 768–773.